NASA/TM-20260009832



Study of Ground Infrastructure to Enable Optical Communications for Deep Space

Yousef K. Chahine, Brian E. Vyhnalek, Jennifer Downey, and Sarah A. Tedder
Glenn Research Center, Cleveland, Ohio

October 2026

NASA STI Program Report Series

Since its founding, NASA has been dedicated to the advancement of aeronautics and space science. The NASA scientific and technical information (STI) program plays a key part in helping NASA maintain this important role.

The NASA STI program operates under the auspices of the Agency Chief Information Officer. It collects, organizes, provides for archiving, and disseminates NASA's STI. The NASA STI program provides access to the NTRS Registered and its public interface, the NASA Technical Reports Server, thus providing one of the largest collections of aeronautical and space science STI in the world. Results are published in both non-NASA channels and by NASA in the NASA STI Report Series, which includes the following report types:

- TECHNICAL PUBLICATION.
  Reports of completed research or a major significant phase of research that present the results of NASA programs and include extensive data or theoretical analysis. Includes compilations of significant scientific and technical data and information deemed to be of continuing reference value. NASA counterpart of peer-reviewed formal professional papers but has less stringent limitations on manuscript length and extent of graphic presentations.

- TECHNICAL MEMORANDUM.
  Scientific and technical findings that are preliminary or of specialized interest, e.g., quick release reports, working papers, and bibliographies that contain minimal annotation. Does not contain extensive analysis.

- CONTRACTOR REPORT.
  Scientific and technical findings by NASA-sponsored contractors and grantees.

- CONFERENCE PUBLICATION.
  Collected papers from scientific and technical conferences, symposia, seminars, or other meetings sponsored or cosponsored by NASA.

- SPECIAL PUBLICATION.
  Scientific, technical, or historical information from NASA programs, projects, and missions, often concerned with subjects having substantial public interest.

- TECHNICAL TRANSLATION.
  English-language translations of foreign scientific and technical material pertinent to NASA's mission.

Specialized services also include organizing and publishing research results, distributing specialized research announcements and feeds, providing information desk and personal search support, and enabling data exchange services.

For more information about the NASA STI program, see the following:

- Access the NASA STI program home page at http://www.sti.nasa.gov

NASA/TM-20260009832



Study of Ground Infrastructure to Enable Optical Communications for Deep Space

Yousef K. Chahine, Brian E. Vyhnalek, Jennifer Downey, and Sarah A. Tedder
Glenn Research Center, Cleveland, Ohio

National Aeronautics and
Space Administration

Glenn Research Center
Cleveland, Ohio 44135

October 2026

Acknowledgments

This work was funded by NASA's Science Mission Directorate. We would like to thank Bernie Edwards and Carolyn Mercer for their suggestions.

This report contains preliminary findings, subject to revision as analysis proceeds.

Trade names and trademarks are used in this report for identification only. Their usage does not constitute an official endorsement, either expressed or implied, by the National Aeronautics and Space Administration.

Level of Review: This material has been technically reviewed by technical management.

This report is available in electronic form at https://www.sti.nasa.gov/ and https://ntrs.nasa.gov/

NASA STI Program/Mail Stop 050
NASA Langley Research Center
Hampton, VA 23681-2199

Study of Ground Infrastructure to Enable Optical Communications for Deep Space

Yousef K. Chahine, Brian E. Vyhnalek, Jennifer Downey, and Sarah A. Tedder

NASA Glenn Research Center, Cleveland, Ohio, 44135

ABSTRACT

Deep space optical communication systems offer the promise of significantly higher data return compared to traditional RF systems and the potential for less congested communication networks for operations at distances greater than 1M km. NASA missions would benefit from the adoption of optical communications for deep space not just for the higher data rates on individual missions but also because it would reduce dependence on the already over-subscribed Deep Space Network (DSN) system and therefore benefit a whole suite of missions. Successful high data rate optical communications have been demonstrated by NASA's Laser Communications Relay Demonstration (LCRD), the Lunar Laser Communications Demonstration (LLCD), Deep Space Optical Communications (DSOC). However, the use of optical communications is not currently available to our deep space missions from cislunar space and beyond because the necessary ground infrastructure is not in place. Because optical communication cannot be adopted for deep space missions without this infrastructure, this study provides a description of what such a ground infrastructure might look like, using performance data for technologies developed under the NASA's projects such as the Real Time Optical Receiver (RealTOR), the Low Cost Optical Terminal (LCOT), and DSOC. These technologies are used as a basis to design a ground station that can provide 5 times better data rates from Uranus than those predicted when using RF.

Keywords: optical communications, deep space, laser communications

1. INTRODUCTION

Deep space optical communication systems offer the promise of significantly higher data return compared to traditional RF systems and the potential for less congested communication networks for deep space missions. The adoption of optical communication for deep space would reduce dependence on the already over-subscribed Deep Space Network (DSN).

Currently the deep space downlink capability is covered by the DSN. Mars orbiters, transmitting from 2.5 AU from the Earth, typically transmit at about 500 kbps, and the data downlink from a few days of observation of Pluto by New Horizons took two years.

Optical communications demonstrations in cislunar and deep space show that better performance is possible. Successful high data rate optical communications have been demonstrated by NASA's Laser Communications Relay Demonstration (LCRD), the Lunar Laser Communications Demonstration (LLCD), and Deep Space Optical Communications (DSOC). DSOC has successfully downlinked at a rate of 8 Mbps from 3 AU. However, the use of optical communications is not available to our deep space missions from cislunar space and beyond because the necessary ground infrastructure has not been built.

This study focuses on the potential design of an optical communications ground infrastructure using performance data from a modular COTS-based technology developed under the NASA RealTOR, LCOT, and DSOC projects. The goal is to receive data at 5 times better data rates (100 kbps) from Uranus as compared to expected Uranus Orbiter Probe (UOP) performance detailed in the "Uranus Orbiter and Probe" study submitted to the Planetary Science Decadal Survey on June 7, 2021. In this previous study the Ka-band downlink communications system transmits data at a rate of 19.5 kbps using a 100 Watt (58 W RF) traveling wave tube amplifier (TWTA) and a 3.1-meter high gain antenna. Data would be downlinked during an 8 hour pass once a week during the cruise phase, and data would be downlinked during an 8 hour pass once a day during the tour. A total of 70.2

*yousef.k.chahine@nasa.gov; phone 1 216 433-6649; www.nasa.gov

kB of data would be downlinked each pass. The UOP Ka-band and X-band communications systems have a combined mass of 92.4 kg and use 118 watts at a time.

In this study, we propose the strategy of using an array of smaller aperture optical telescopes for the ground infrastructure. This allows the use of commercial-off-the-shelf (COTS) telescopes similar to the LCOT design to reduce development needs and costs compared to ground stations using custom large aperture telescopes. This study focuses on the use of RealTOR technology which is introduced in Section 2. Details such as the number and size of telescopes as well as transmitter power and size requirements are presented in Section 3. The key development needed for the RealTOR technology to support the telescope array strategy is the combination of signals from multiple apertures. Figures 1 and 2 show two possible concepts for array signal combining whose benefits and challenges are discussed in Section 4. The number of ground stations and site selection recommendations are presented in Section 5. The timeline and development path for the establishment of the ground infrastructure is presented in Section 6. Finally, in Section 7, we summarize several point designs and discuss future work.

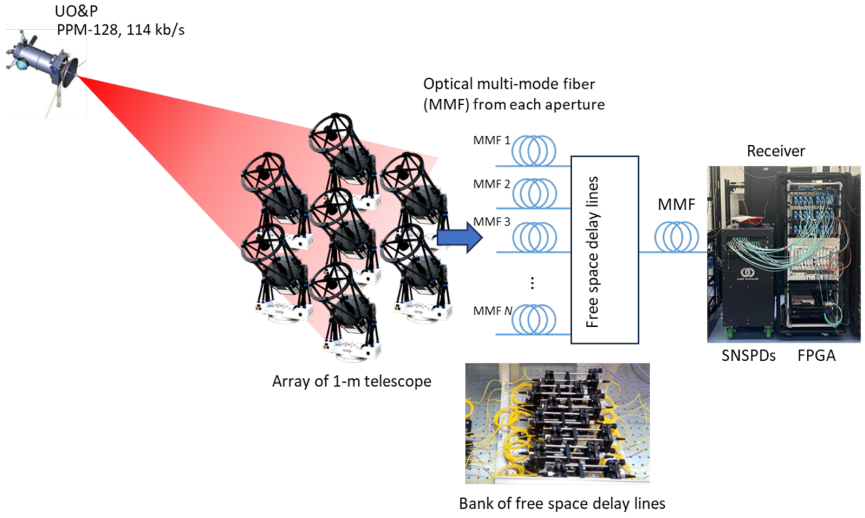


Figure 1: Conceptual drawing of the optical ground telescope array with optical signal combining.

2. REALTOR RECEIVER SYSTEM OVERVIEW

The receiver system consists of a fiber interconnect, superconducting nanowire single photon detectors (SNSPDs), and an FPGA-based receive modem. Light from the backend optics of the telescope is coupled into the receiver system at the fiber interconnect which efficiently delivers light to the SNSPDs. The modem performs demodulation and decoding.

Two fiber interconnect/detector architectures were prototyped and tested in the laboratory. The first architecture, shown in Fig. 3, consists of a photonic lantern with a 55 μm core diameter input supporting 70 modes and seven few-mode fiber (FMF) output legs. Each FMF is graded-index, has a 25 μm core, and supports the first 10 linearly polarized (LP) modes per polarization counting parity. Each output leg is butt-coupled to a FMF with a graded index 20 μm diameter supporting 6 LP modes. Each of these fibers are then butt-coupled to a single-pixel SNSPD. The single-pixel SNSPD output pulses have a rise time of about 850 ps and a 1/e reset time on the order of 15 ns.

The second architecture, shown in Fig. 4, consists of a 25 μm single FMF (10 LP modes) coupled to a graded-index 20 μm diameter FMF supporting 6 LP modes. This fiber is butt-coupled to the 16-channel SNSPD array. The array output pulse rise times are on average 500 ps, with 1/e reset times in the 5 - 8 ns range.

The FPGA-based receive modem is implemented on two COTS FPGA cards housed in a Micro Telecommunications Architecture (MicroTCA) chassis. The radio frequency system on a chip (RFSoC) FPGA samples the

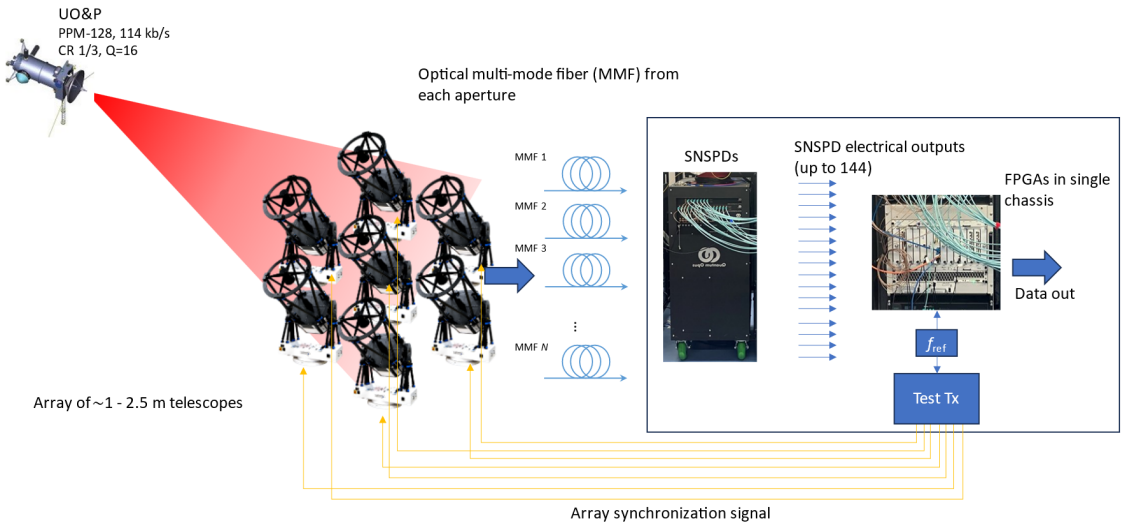


Figure 2: Conceptual drawing of the optical ground telescope array with digital signal combining.

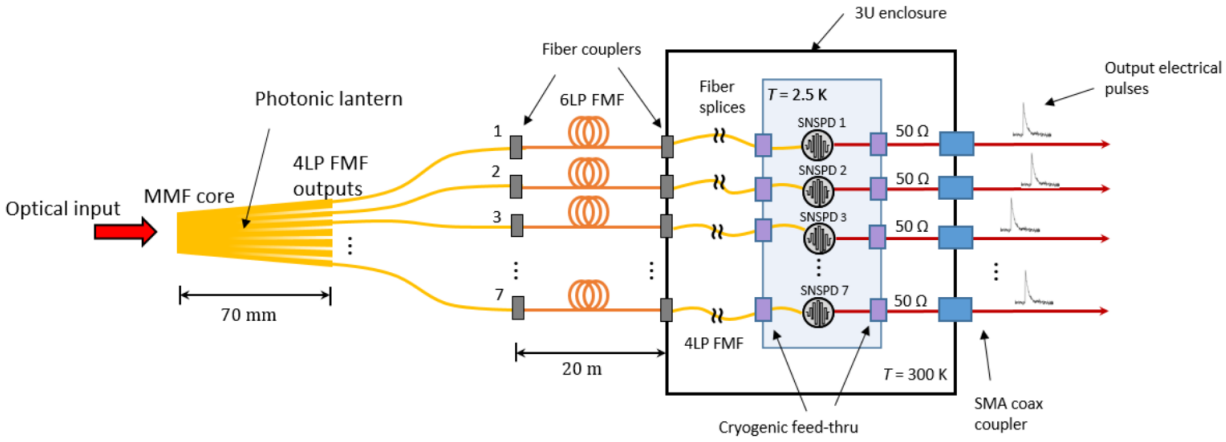


Figure 3: Schematic of the 7-leg photonic lantern coupled SNSPD subsystem.

detector pulses with 16 analog to digital converters at a sample rate of 2 GHz. It also performs detector channel alignment and combining, symbol timing recovery, codeword alignment, and symbol deinterleaving. The second FPGA card is used for iterative decoding, derandomization and deslicing.

The fiber interconnect/detector architectures and the FPGA-based modem from the RealTOR project will serve as the basic building blocks for the proposed telescope array architecture.

3. LINK BUDGET

The link budget provides a framework in which to evaluate if a given link can support a target data rate. The data rate power and signal-to-noise requirements are based on the bit error probability of serially concatenated pulse position modulation (SCPPM) evaluated for a Poisson channel under varying levels of background flux. An overview of basic assumptions present in the link budget is presented before the results. In general, the link figure of merit is calculated as the ratio of the power received P_r, to the power required P_{req} to achieve the desired data rate with an acceptable level of bit error. The power received is determined from the transmitter

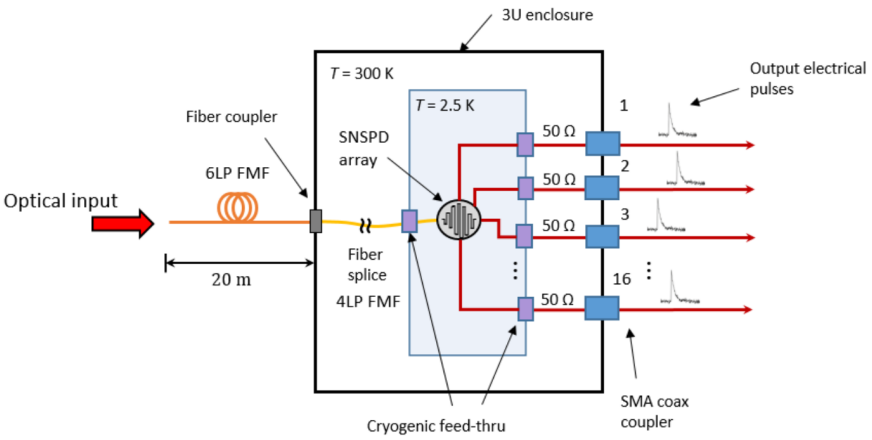


Figure 4: Schematic of the FMF coupled 16-channel SNSPD array subsystem.

power and gain together with the receiver gain while accounting for various losses in the system

$$P_r = P_t G_t G_r L_s L_{\text{atm}} L_{\text{pt}} \eta_t \eta_r, \tag{1}$$

where P_t is the transmitted power, G_t is the transmitter gain, G_r is the receiver gain, L_s is the space loss, L_{atm} is atmospheric loss, L_{pt} is the pointing loss, and η_t and η_r are the transmitter and receiver efficiencies. Similarly, the required power is determined from the minimum power needed to close the link for a lossless receiver and then accounting for the receiver system losses. The power required at the fiber interconnect is given by

$$P_{\text{req}} = P_i / \left(L_b L_f \eta_{\text{det}} \eta_{\text{fib}} \eta_{\text{imp}} \right) \tag{2}$$

where P_i is the minimum power required based on SCPPM code performance, L_b is the detector blocking loss due to count rate saturation, L_f is a fade loss due to effects such as atmospheric scintillation and transmitter pointing jitter, η_{det} is the single photon detector efficiency, η_{fib} is the fiber coupling efficiency from the telescope, and η_{imp} is the processing electronics implementation efficiency. Finally, the link margin, $M = P_r / P_{\text{req}}$, provides the link feasibility with $M \geq 0$ dB defining a closed link and $M < 0$ dB a failed communication link. While the values used in the calculation are typically for an average worst-case, depending on knowledge of system components and atmospheric effects there is uncertainty such that generally a few dB of margin may be allocated to the link evaluation to accommodate potential unknowns.

3.1 Example Link Budget

In this section, we walk through an example link budget for a PPM-128 mode with 8 ns slot and symbol repeat 16 for a 114 kbps link from 19.3 AU, summarizing our key assumptions. In this example, we consider a ground station consisting of an array of 70 cm telescopes matched to current RealTOR hardware with minimal additional development. In Section 3.2, we present a general analysis which summarizes the reduction in spacecraft transmitter size, weight, and power requirements that can be achieved with reasonable additional ground station and receiver development.

3.1.1 Transmitter

We assume a transmission wavelength of 1550 nm, and restrict our attention to transmit telescope apertures of 22 cm, 30 cm and 50 cm. The 22 cm baseline is based on the DSOC transmitter and thus requires minimal additional development. The 50 cm aperture is motivated by the High-Resolution Imaging Science Experiment (HiRISE) optical imaging telescope used for the Mars Reconnaissance Orbiter (MRO) mission and thus has a spaceflight-ready design baseline, although such a transmitter would require a complete, independent design as part of an optical communications terminal, in particular to meet the strict pointing requirements imposed by

the reduced beam divergence. We assume all transmit telescopes use an off-axis design without central obscuration. It is assumed that pointing can be achieved within a 1.07 dB average pointing loss, corresponding to a 2.5 μrad pointing offset for the 22 cm aperture, reducing to a 1.1 μrad pointing requirement for the 50 cm transmit aperture.

Transmitter Gain

The transmitter gain is given by [1]

$$G_t = \left(\frac{4\pi A}{\lambda^2}\right) g_t(\alpha, \beta, \gamma, X) \tag{3}$$

where A is the primary aperture area, λ is the wavelength, and α, β, γ, X are dimensionless parameters. The first term $4\pi A/\lambda^2$ represents the ideal aperture gain, while the function $g_T(\alpha, \beta, \gamma, X)$ is the deviation from ideal due to beam width, wavefront curvature, central obscuration, etc., as well as defining the angular beam pattern. In general, $g_t(\alpha, \beta, \gamma, X)$ is defined by

$$g_t(\alpha, \beta, \gamma, X) = 2\alpha^2 \left| \int_{\gamma^2}^{1} \exp(j\beta u) \exp(-\alpha^2 u) J_0\left[X(u)^{1/2}\right] du \right|^2 \tag{4}$$

where $\alpha = a/\omega$ is the ratio of the primary aperture radius to the $1/e^2$ beam width, quantifying truncation by the aperture, $\gamma = b/a$ is the secondary to primary mirror obscuration ratio, $\beta = (ka^2/2)[(1/r) + (1/R)]$ parameterizes near field and focusing effects, k is the wavenumber, R is the radius of curvature, r is a field point, and $X = ka \sin\theta$ parameterizes the off-axis dependence. Figure 5 shows a transmitter schematic and normalized gain patterns for $a = 22$ cm and $a = 50$ cm with $\gamma = 0$.

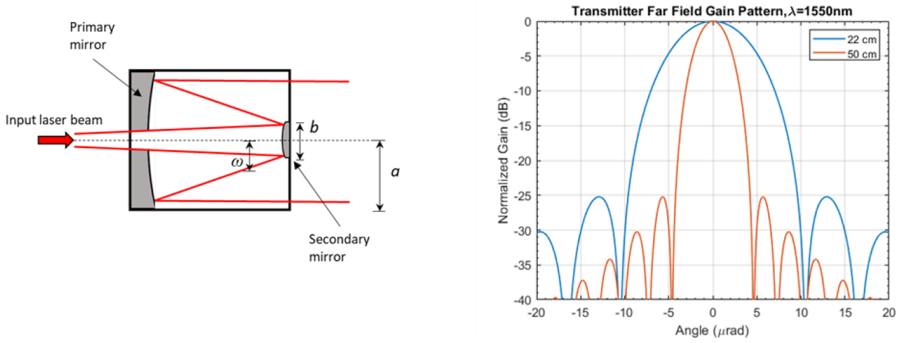


Figure 5: Transmitter schematic (left), and far field gain pattern (right).

For on-axis gain $X = 0$, and far-field $\beta \to 0$, g_t reduces to

$$g_t(\alpha, 0, \gamma, 0) = \frac{2}{\alpha^2}\left[\exp(-\alpha^2) - \exp(-\gamma^2\alpha^2)\right]^2 \tag{5}$$

and assuming no obscuration ($\gamma = 0$), g_t further reduces to

$$g_t(\alpha, 0, 0, 0) = \frac{2}{\alpha^2}\left[\exp(-\alpha^2) - 1\right]^2 \tag{6}$$

with the optimal beamwidth to aperture ratio given by $\alpha \approx 1.12 - 1.30\gamma^2 + 2.12\gamma^4$, thus $\alpha \approx 1.12$ for $\gamma = 0$. It follows that in this case, the maximum aperture efficiency is $g_t \approx 81.45$ percent, or -0.89 dB. Finally, we calculate the on-axis equivalent isotropic radiated power (EIRP) as is commonly done for RF antennas as:

$$\text{EIRP} = P_t G_t L_p \eta_t \tag{7}$$

where the transmitter efficiency η_t includes aperture efficiency as well as all other transmit losses.

Modulation

The transmitter will use photon efficient signaling and implement the CCSDS High Photon Efficiency (HPE) standard, which uses pulse-position modulation (PPM) with variable modulation orders, M = {4, 8, 16, 32, 64, 128, 256} and signal slot widths, $\tau = \{0.5, 1, 2, 4, 8\}$ ns, etc. Signal modulation using PPM is advantageous due to the high peak to average power ratio, which is desirable for deep space communications, and with SCPPM can achieve near-capacity performance. However, imperfect extinction of the laser in non-signal slots reduces the peak-to-average ratio leading to both a reduction in signal power as well as contributing to received background noise photons. The extinction ratio σ_{ER} quantifies the ratio of the laser peak power in the 'on' slot versus the residual power in the 'off' slot, and the peak-to-average power relationship is calculated from

$$P_{\mathrm{avg}} = \frac{1}{T}\int_0^T p(t)dt = \frac{1}{T}\int_0^\tau P_{\mathrm{peak}}dt + \frac{1}{T}\int_0^T \frac{P_{\mathrm{peak}}}{\sigma_{\mathrm{ER}}}dt \tag{8}$$

$$= P_{\mathrm{peak}}\left\{\left(\frac{\tau}{T}\right) + \frac{1}{\sigma_{\mathrm{ER}}}\left[1 - \left(\frac{\tau}{T}\right)\right]\right\} \tag{9}$$

where T is a symbol duration and τ is the slot width. It follows that the peak-to-average ratio is

$$\frac{P_{\mathrm{peak}}}{P_{\mathrm{avg}}} = \left\{\left(\frac{\tau}{T}\right) + \frac{1}{\sigma_{\mathrm{ER}}}\left[1 - \left(\frac{\tau}{T}\right)\right]\right\}^{-1} \tag{10}$$

or

$$\frac{P_{\mathrm{peak}}}{P_{\mathrm{avg}}} = \frac{N}{1 + \sigma_{\mathrm{ER}}^{-1}(N-1)} \tag{11}$$

in terms of PPM slots, $N = (M+G)$, where M is the PPM order, G is the number of guard slots, typically $M/4$, and $T = N\tau$. For PPM-128, the ideal peak-to-average ratio is 160, or 22.04 dB. We assume a 35 dB extinction ratio corresponding to an average signal power reduction of ∼0.21 dB and contributes an average noise power of $\approx P_{\mathrm{avg}}/\sigma_{\mathrm{ER}}$.

The 12 W transmit power in this example is three times the 4 W transmit power of the DSOC space terminal. This is assumed in this example to demonstrate the requirements for a 70 cm receiver telescope array with at most 144 detector channels, consistent with current LCOT and RealTOR hardware (*cf.* Section 4.1). A full analysis of the trade-off between transmitter and receiver requirements is given in Section 3.2.

	Link parameter	Input		Output		Gain		Power	
Transmitter	Wavelength	1550	nm	1.94E+14	Hz				
	Modulation order	128		128					
	Slot period	8	ns	8.00E-09	s				
	Symbol repeats	16	-	16	-				
	Extinction ratio	35	dB	35.00	dB				
	Average power	12	W	40.79	dBm			40.79	dBm
	Aperture diameter	22	cm	0.22	m				
	Ideal aperture gain					112.98	dB		
	Obscuration	0	cm	0.00	ratio				
	Aperture efficiency					-0.89	dB		
	Total pointing loss	1.07	dB			-1.07	dB		
	Other misc. transmitter losses	2.3	dB			-2.30	dB		
	EIRP (on-axis)							149.52	dBm-i

Figure 6: Example link budget (Tx).

3.1.2 Channel

The space loss accounts for the geometric spread of light with distance in the far-field and is defined as

$$L_s = \left(\frac{\lambda}{4\pi R}\right)^2 \tag{12}$$

where R is the range and λ is the wavelength. This term accounts for the largest loss in the system. Since the receiver will be located on Earth, atmospheric transmission must also be considered. Atmospheric transmission is highly dependent on wavelength due to interactions with aerosols and gas molecules scattering or absorbing light, and is similarly dependent on visibility range and altitude. We assume a mid-latitude summer atmospheric model and desert aerosol model at 1 km altitude with visibility of 23 km and 5 km, which gives a zenith transmittance of 92.4 and 80.7 percent, respectively at $\lambda \approx 1550$ nm (Figure 7).

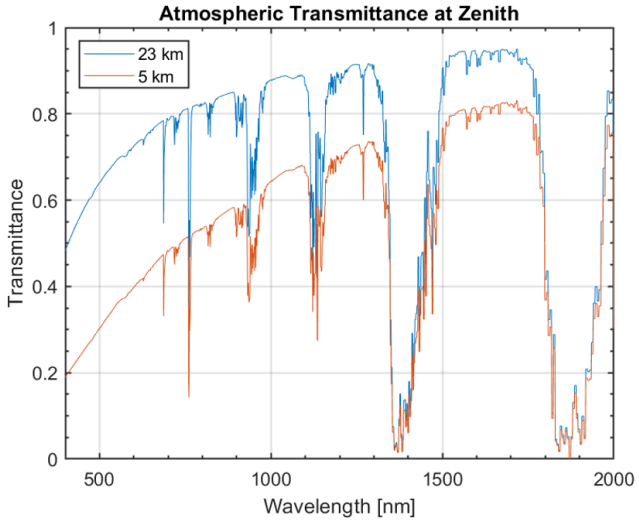


Figure 7: Wavelength dependance of atmospheric transmission.

For lower elevation angles, the relative airmass scales as $\sec\theta$, where θ is the angle from zenith, and the transmission loss is calculated by

$$T = T_0^{\sec\theta}, \tag{13}$$

hence for low elevations such as 30° we expect transmission losses in range of $\approx 0.7 - 1.7$ dB. Here we note the Fried parameter, or coherence length, r_0 which characterizes the spatial scale of atmospheric turbulence. Losses associated with laser propagation through turbulence primarily affect coupling into fiber optics and are discussed in Section 3.1.4.

	Link parameter	Input		Output		Gain		Power	
Channel	Range	2.887E+09	km	2.89E+12	m				
	Space loss					-387.39	dB		
	Power at top of atmosphere							-237.87	dBm
	Atmospheric zenith transmittance	92.4	%	0.92					
	Elevation angle from receiver	30.00	deg	0.52	rad				
	Atmospheric attenuation loss					-0.69	dB		
	Fried parameter, r0	5.00	cm	0.05	m				
	Total channel loss					-388.07	dB		

Figure 8: Example link budget (channel).

3.1.3 Receiver

We consider ground architectures consisting of 70 cm, 1 m, and 2.5 m telescopes, respectively. The 70 cm telescope corresponds directly to the LCOT ground station and can be matched to the RealTOR fiber-detector subsystem with only minor additional detector development needed to increase the size of the fiber used internally by the COTS SNSPDs. The 1 m corresponds to a commercially available telescope very similar to the 70 cm model and would thus require minimal ground station redesign to adapt the current LCOT blueprint. The 2.5 meter is based on a commercially available telescope, but the larger aperture ground station would require the most additional design and development relative to an LCOT-like ground station, and may limit the minimum operational Sun-Earth-Probe (SEP) angle to prevent direct sunlight/internal heating from degrading critical optical elements.

	Link parameter	Input		Output		Gain		Power	
Receiver	Received power on ground							-238.56	dBm
	Aperture diameter	70	cm	0.70	m				
	Ideal aperture gain					123.04	dB		
	Obscuration diameter	19	cm	0.19	m				
	Aperture efficiency			0.93		-0.33	dB		
	Average pointing and tracking loss	1	dB			-1.00	dB		
	Other misc. receiver losses	3	dB			-3.00	dB		
	Array size	18	-	18	-	12.55	dB		
	Average received power (dBm)							-107.30	dBm

Figure 9: Example link budget (Rx).

3.1.4 Fiber interconnect

We assume a fiber-coupled detector system without adaptive optics or atmospheric tilt compensation. The link budgets assume worst-case daytime turbulence with Fried parameter $r_0 = 5$ cm at 1550 nm and 30° elevation, corresponding to an atmospheric coherence ratio D/r_0 of 14, 20, and 50 for the 70 cm, 1 m and 2.5 m receiving apertures, respectively. As discussed below, to maximize power-in-fiber we do not assume any atmospheric tilt compensation or adaptive optics, minimizing the amount of light that must be diverted to run the tracking system.

	Link parameter	Input		Output		Gain		Power	
Fiber	Fiber core diameter	100	µm	1.00E-04	m				
	Fiber input NA	0.22	-						
	Number of GRIN fiber modes			249.00	modes				
	Total coupling loss					-1.92	dB		
	Power in fiber (PIF)							-109.22	dBm

Figure 10: Example link budget (fiber interconnect).

The fiber insertion loss is based on a model for the coupling efficiency to mode-limited fiber devices without tilt-correction which has been verified against in-lab and on-sky fiber measurements and is given by [2]

$$\eta_{\text{fib}} = 0.822(1 - e^{-3\Sigma^2}) \tag{14}$$

where the efficiency parameter Σ^2 is based on the number of supported fiber spatial modes M according to

$$\Sigma^2 = \frac{4}{\pi^2} \cdot \frac{M}{(1 + (D/r_0)^{5/3})^{6/5}}. \tag{15}$$

Fig. 11 shows the dependence of the coupling loss on the number of fiber modes for the assumed worst-case turbulence conditions with each telescope aperture. Note that Eq. (14) assumes a minimum of at least 0.8

dB coupling loss; lower coupling loss can be achieved with careful attention to optical tolerances as shown in the figure. Combined with other design considerations presented in Section 4.2, we assume a system capable of supporting 249 spatial modes (per polarization) matched to the 70 cm aperture, 525 spatial modes matched to the 1 m aperture, and 3125 spatial modes matched to the 2.5 m aperture, yielding an estimated coupling loss less than 2 dB in worst-case daytime turbulence over low-elevation paths. Other specifics of these fibers are discussed in Section 4.2. The turbulence-induced coupling loss can potentially be improved with additional SNSPD development to support efficient coupling to larger fibers; however, for links where the dominant noise source is background light (typically lower data rate modes with long slot widths), reducing the coupling loss below 2 dB comes at the cost of reduced SNR, since the marginal gain in coupling efficiency introduces additional background light proportional to the number of fiber modes. In Fig. 11, it can be seen that below 2 dB coupling loss the number of modes (and hence background light) begins to scale faster than the additional signal obtained via the improved coupling efficiency. Thus, although low-noise links with enough SNR can benefit from maximizing the coupling efficiency to reach higher data rates, the associated reduction in SNR will constrain the lowest data rate link than can be achieved by the array as detailed in Sec. 3.4.

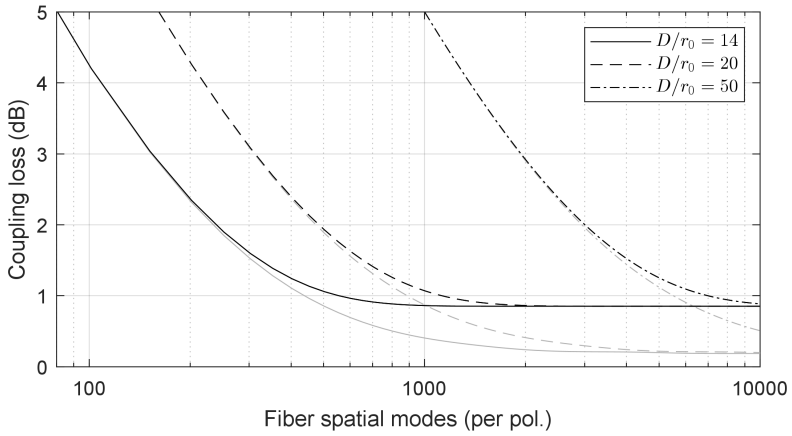
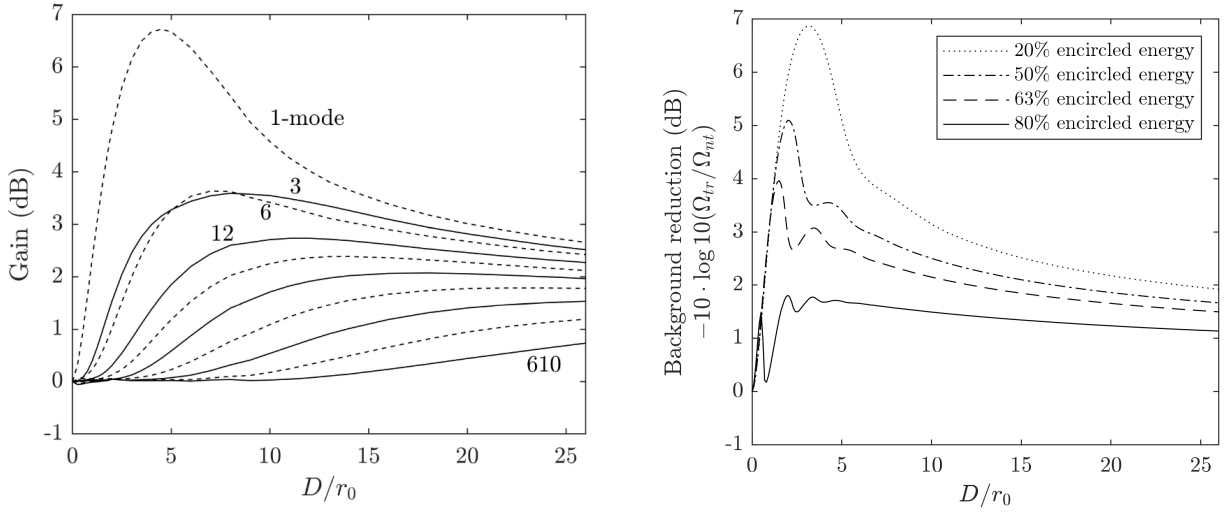


Figure 11: Dependence of fiber coupling efficiency on total number of guided modes, assuming worst-case turbulence $D/r_0 = 14$, 20, and 50, for the 70 cm, 1 m, and 2.5 m apertures, respectively. The darker curves show the approximation (14) used in the link budget and the lighter curves show an approximation from [2] which is more accurate for high-efficiency coupling.

In contrast to the current RealTOR system which requires coupling to few-mode fibers, the larger fiber assumed for the UOP ground station mitigates the need for high-speed closed loop tracking to compensate tilt from atmospheric turbulence. To quantify this, Figure 12a shows the gain obtained from atmospheric tilt compensation on fiber coupling efficiency [2]. Note that as the number of fiber modes increases, the gain from high-rate closed loop tracking is less substantial. Thus, when operating a fiber-coupled receiver with the very low power level expected from a UOP link (below -100 dBm for a 1 m aperture), the gain provided for fibers with more than ∼150 modes is likely offset by the additional light diverted to run the tracking loop at the high-rates (∼200-600 Hz) required for atmospheric tilt compensation. For this study, the fiber interconnect is assumed to operate with only low-rate tracking, and is specified to support enough modes to obtain the required coupling efficiency without adaptive optics or compensation for atmospheric tilt.

One caveat of this assumption is that a design targeting a prescribed coupling efficiency at a nominal operating turbulence condition D/r_0 will require a larger fiber relative to a system which provides atmospheric tilt compensation. Figure 12b shows the reduction in the solid-angle field-of-view Ω required to capture a fixed percentage of light from an atmospherically-distorted point source when atmospheric tilt compensation is employed, based on numerical calculations of the point spread function described in [3]. This reduction is roughly equal to the reduction in the number of fiber modes required to couple the light in the focal plane of the telescope and hence is also proportional to the reduction in uniform background light coupled to the detectors. For example,

assuming a system targeting 2 dB coupling loss (63% efficiency) at $D/r_0 = 14$, a fiber interconnect designed with atmospheric tilt compensation can suppress the background by 1.9 dB. The achievable background suppression decreases as the assumed operating turbulence condition increases (e.g., to support a larger telescope). Thus, just as the gain in coupling efficiency from atmospheric tilt compensation becomes less pronounced for systems designed for severe turbulence conditions, the achievable background suppression also becomes less significant.



(a) (b)

Figure 12: (a) Gain in coupling efficiency from atmospheric tilt compensation for fibers with (from top to bottom) 1, 3, 6, 12, 23, 42, 78, 154, 297, and 610 guided spatial modes (per polarization). Dashed and solid lines are used only for contrast between curves. (b) Reduction in solid angle field-of-view (FOV) required to capture a fixed encircled energy ratio from an atmospherically distorted point source when atmospheric tilt compensation is employed (characterizes suppression of uniform background light achievable with atmospheric tilt compensation).

3.1.5 Background

Estimates for sky radiance at wavelengths near 1550 nm generally range from $I_\nu \simeq 10^{-8}$ W/(cm^2 sr μm) at night to around $I_\nu \simeq 2.5 \cdot 10^{-3}$ W/(cm^2 sr μm) in worst-case sunshine.[4] The latter background radiance imposes restrictions on the operation of the lowest data rate modes (i.e. 114 kbps). For the current example, we consider nighttime operation at a twilight sky radiance of $I_\nu = 10^{-6}$ W/(cm^2 sr μm) and postpone a complete discussion of background limits to Section 3.4.

Only the modes accepted by the fiber are coupled to the detectors, and so the spectral radiance I_ν is converted to the photon mean occupation number μ_b (photons/mode) via the conversion $\mu_b = I_\nu c^3/(h\nu^5)$ [5], which is then converted to the flux on the detectors based on the number of (spatial) modes M per polarization per time-frequency mode collected by the fiber, times the number of filtered time-frequency modes per second, given by $1/\Delta t = \Delta\nu$ assuming a bandpass filter of bandwidth $\Delta\nu$, yielding the total background flux $\Phi_b = \mu_b M \Delta\nu$. The transmitter noise flux is calculated based on the signal flux on the detectors and the transmitter extinction ratio over all non-signal slots.

3.1.6 Detectors

The detector specification is based on the need to efficiently couple the required number of spatial modes while maintaining sufficiently low jitter and high count rate to support higher data rates where power permits. Although the lower data rates assumed for Uranus link ranges put minimal requirement on the total number of detector channels and count-rate, we instead base the count-rate requirement on operation at Mars-like distances with higher data rates to support more general use of the ground architecture as well as use during the initial UOP cruise phase. A second constraint on the number of detectors needed to support the telescope array is

	Link parameter	Input		Output		Gain		Power	
Background	Sky radiance	1.0E-06	W/(cm2 sr µm)	1.00E-06	W/(cm2 sr µm)				
	Stray radiance	1.00E-09	W/(cm2 sr µm)	1.00E-09	W/(cm2 sr µm)				
	Bandpass filter bandwidth	0.10	nm	1.25E+10	Hz				
	Total background flux			1.21E+05	ph/s				
	Received transmitter noise photon flux			5.34E+03	ph/s				
	Total received noise photons per slot			0.00075	ph/slot				

Figure 13: Example link budget (background).

imposed by the total detection area required to collect light from $M \sim (D/r_0)^2$ spatial modes per telescope. The detectors can efficiently couple $M \sim A\Omega/\lambda^2$ modes depending on the product of total detection area A and maximum solid angle Ω of the supporting cavity relative to the fundamental phase space volume λ^2 of a single spatial mode.

With existing RealTOR COTS SNSPDs, a 50-micron array developed under a NASA SBIR has 16 detector channels covering an area 50 μm in diameter. To support coupling to a graded-index fiber carrying at least ~250 spatial modes, we assume a 100 μm detection area coupled to each 70 cm telescope. The total number of channels per unit area must also be reduced relative to the current RealTOR SNSPDs to support larger telescope arrays. For this study, we assume SNSPDs can be developed with 8 detector channels per 100 μm area, increasing the area that must be covered by each nanowire by a factor of 8 relative to existing RealTOR COTS SNSPDs. Since kinetic inductance of the SNSPDs scales with length, this is expected to increase the reset time of the detectors to ~60 ns; reducing the maximum count rate of each detector to ~3 Mcps. This is more than sufficient for data rates achievable for deep space links, although it limits the peak data rates for near-earth links to several hundred Mbps assuming up to 144 total detector channels (Section 4.1). Additional requirements to support a 1-m array and 2.5-m array are discussed in Section 3.2.

	Link parameter	Input		Output		Gain		Power	
SNSPDs	Dark count rate per detector	200	cts/s	2.00E+02	cts/s				
	Detector efficiency	70.00	%	0.7000		-1.55	dB		
	Detector 1/e reset time	60	ns	6.00E-08	s				
	Number of detectors per telescope	8		8					
	Total number of detectors			144					
	Blocking loss					0.000	dB		
	Total detected *Ks*							1.3388	cts/slot
	Total detected *Kb*			0.00878	cts/slot				

Figure 14: Example link budget (detectors).

3.1.7 Decoder and timing recovery loop

The link budget is required to yield a positive link margin based on K_s/M requirements for SCPPM code performance with implementation loss for each PPM mode obtained from in-lab testing of the RealTOR system. The budget is also required to yield a positive tracking margin for the timing recovery loop (TRL) based on a minimum required K_s of 0.05 cts/signal slot obtained from RealTOR receiver testing. For arrays of non-coplanar receive apertures, the timing recovery algorithm must be able to track slot phase differences between array elements which change with the alt.-az. angles of the array, which is not a current requirement of the RealTOR TRL, and may have an effect on the minimum required K_s needed for timing recovery. A full analysis of the signal requirements for array timing recovery is postponed to Section 3.3. A 1 dB implementation loss $\eta_{\text{imp},0} = 0.79$ is assumed for background/dark counts below $K_b = 0.01$, based on RealTOR receiver test results. For K_b between 0.01 and 0.1, we assume a continuous increase to 2 dB implementation loss based on a degradation of TRL tracking performance for higher order PPM modes observed in system testing. It is assumed that the background counts per slot cannot exceed $K_b \sim 0.1$ for $K_s \sim 1$, due to degradation of TRL tracking performance

for higher order PPM modes. This is modeled by a steep increase in implementation loss $\eta_{\text{imp}} = \eta_{\text{imp},0}^{\exp(K_b/0.15)}$. Fading loss is assumed to be less than 1 dB, consistent with prior testing performed under more severe fading conditions [6].

	Link parameter	Input		Output		Gain		Power	
Totals	Detected *Ks* for TRL							**0.0836**	**cts/slot**
	Minimum *Ks* for TRL	0.05	ph/slot	**0.0500**	**cts/slot**				
	Minimum *Ks* for TRL w/sym repeat							**0.8000**	**cts/clot**
	Tracking margin							2.23	dB
	Detected Ks/M							**-19.81**	**dB-cts/slot**
	Code required signal photons, *Ks/M*	-22.16	dB-ph/slot	**-22.16**	**dB-cts/slot**				
	Decoder implementation loss	1.00	dB			**-1.04**	**dB**		
	Fading loss	1.00	dB			**-1.00**	**dB**		
	Total required signal photons, *Ks/M*							-20.12	dB-cts/slot
	Link margin							0.31	dB

Figure 15: Example link budget (totals).

Note that with this example, based on a replica of the LCOT 70 cm ground station with current RealTOR hardware and very little additional development, a positive link margin for the 114 kbps mode requires an 18-telescope array and a three-fold increase in transmit power compared to the DSOC space terminal. However, with reasonable modifications of the LCOT ground station to support a 1-m telescope array, the required spacecraft transmit power can be significantly reduced as outlined in the next section.

3.2 Transmitter requirements vs. ground station requirements

Based on estimates with current RealTOR hardware, the minimum 3-fold increase in required transmit power (EIRP) compared to the current DSOC space terminal can generally only be achieved through the addition of size/mass (larger transmit aperture) and/or spacecraft power. This assumes minimal development of the RealTOR receiver and LCOT ground station, namely, FPGA development to support 144 detector channels within the current FPGA architecture (Section 4.1), and development of SNSPDs with a larger detection area together with a reduction in dark counts to 200 cps per detector (which can be achieved by detectors with lower operating temperatures and additional filtering). Based on improvements in commercial SNSPD technology over the last 10 years, these modest improvements in the RealTOR detector characteristics would enable the system to support larger arrays and reduce the burden on the spacecraft size, weight, and power.

To support a telescope with a 1 m diameter collecting area, we assume each telescope again couples to a detection area of ∼100 μm diameter, but with a larger acceptance NA of 0.32. Again, we estimate that this can be achieved with 8 detector elements per 1 m aperture, maintaining 70% detection efficiency, 60 ns reset time, timing jitter within 80 ps, and a dark count rate of less than 200 cps per detector element. To support a telescope with 2.5 m aperture we assume a detector with 250 μm diameter and 48 elements (scaling roughly with the area), meeting the same requirements. Note that with these assumptions on the geometry of each detector element, the total number of detector channels scales with the size N of the receiver array as $8N$ for the 70 cm and 1 m arrays and $48N$ for the 2.5 m array.

3.2.1 Transmit power vs. receiver array size. Data rates from 19.3 AU.

Figure 16 shows the dependence of the achievable data rates based on both transmit power and array size for a 70 cm array (left) and a 1 m array (right) using the same assumptions on background/dark counts presented in the link budget above. The number of telescopes scales up to a maximum of 18 before reaching 144 total detector channels supported by the current FPGAs and FPGA architecture. For the 70 cm array, a 114 kbps link from 19.3 AU would then require a 12 W transmit power assuming a 22 cm transmit aperture (A), reducing to ∼6 W for the 1 m array (B).

Of course, the array size requirements can potentially be reduced by further enhancement of the space transmitter. For example, we find that to keep the size of the 70 cm array below $N = 9$, transmitter requirements start at 22 W for the 22 cm transmit aperture (C), reducing to 4 W for a 50 cm transmit aperture (D) assuming

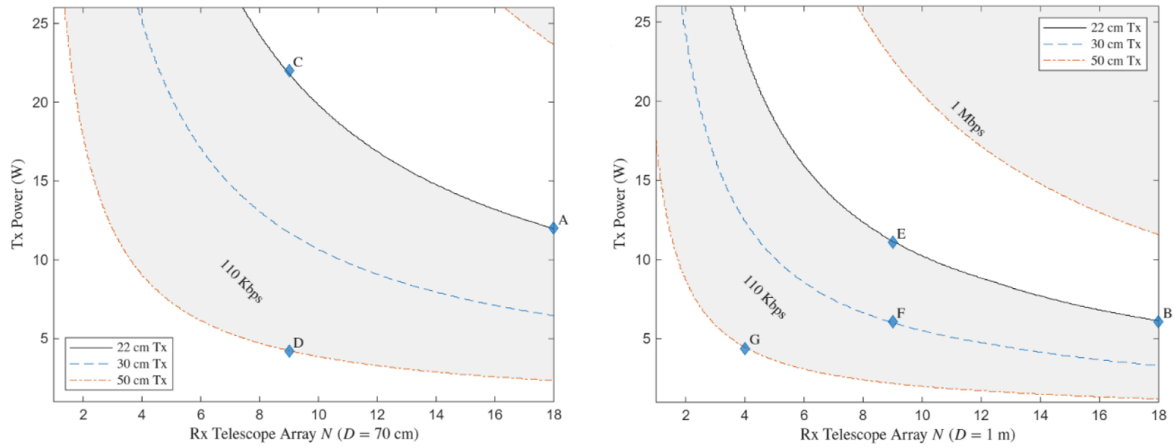


Figure 16: Data rate dependence on transmit power for 70 cm (left) and 1 m (right) arrays from 19.3 AU.

1.1 μrad pointing can be achieved. With a 1-meter 9-telescope array, the transmit power requirement is ∼11 W for the 22 cm transmitter (E), or ∼6 W for a 30 cm transmit aperture (F). Finally, a 4-telescope 1-meter array can close the link with a 5 W transmitter with 50 cm transmit aperture (G).

With a 2.5 m array (Figure 17), both the transmit power and array size can be reduced, achieving the 114 kbps data rate with 3 telescopes assuming a 7 W, 22-cm DSOC-like transmitter (H), or with 2 telescopes and a 5 W, 30 cm transmitter (I). However, it should be noted that the increase in receive aperture size to 2.5 meters requires the most significant ground station development relative to the LCOT blueprint. For daytime operations, the larger aperture may result in stricter limitations on the Sun-Earth-Probe angle relative to the 70 cm or 1-meter ground telescope.

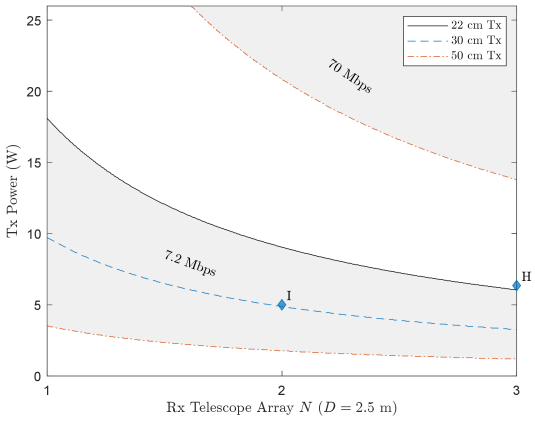


Figure 17: Data rate dependence on transmit power and array size for 2.5 m array from 19.3 AU.

3.2.2 Transmit power vs. receiver array size. Data rates from 2.67 AU (Mars).

In addition to supporting the lowest data rate modes from Uranus distances, the ground stations should support operations from intermediate ranges including high data rates from Mars. Figures 18 and 19 show the achievable data rates from 2.67 AU on the same axes as in the previous section, showing that the same ground station architecture used for 114 kbps from Uranus can also support ∼5-7 Mbps from Mars.

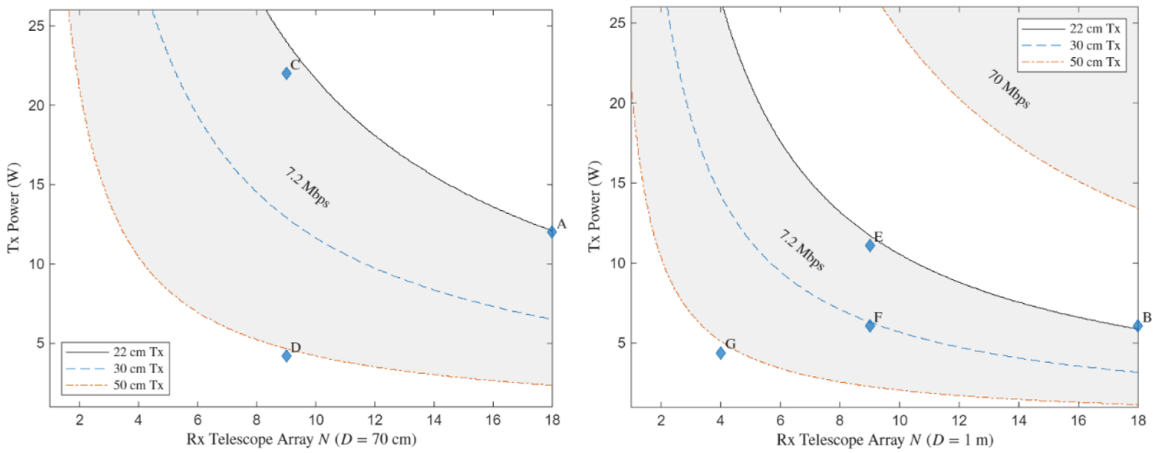


Figure 18: Data rate dependence on transmit power for 70 cm array (left) and 1 m array (right) from 2.67 AU.

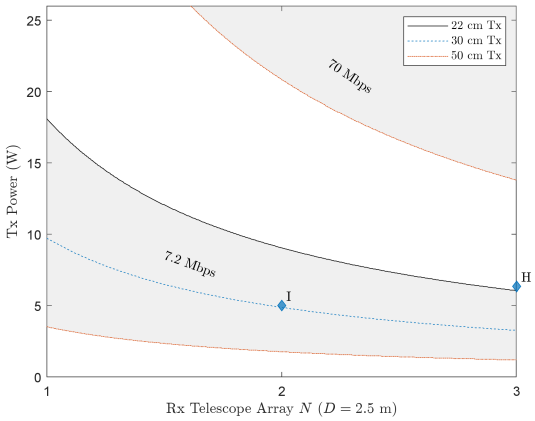


Figure 19: Data rate dependence on transmit power and array size for 2.5-meter array from 2.67 AU.

3.2.3 Transmit power vs. receiver array size. Data rates from 0.01 AU (L1/L2).

It should be noted that there are limitations to employing this architecture at the highest PPM data rates accessible from L1/L2 or cis-lunar link ranges. Specifically, the large area detectors proposed for the UOP ground station architecture can be expected to have longer reset times (60 ns compared to 10 ns with current RealTOR detectors), and thus begin to saturate at ∼3 Mcps per detector, limiting data rates to several hundred Mbps. However, the large array makes these data rates accessible with smaller, low-power transmitters on the spacecraft, as shown in Figure 20 for the 1-meter array.

Note that with a 10 cm transmitter, a 1-meter array with $N = 4$ telescopes achieves 300 Mbps from L2 with ∼350 mW transmit laser power. For a 7.5 cm transmit aperture, the same rate is achieved with a 1 W transmit power. Note that by enabling a smaller transmit aperture, the spacecraft pointing requirement is also relaxed, expanding to 5.5 μrad for the 10 cm aperture, and up to 11 μrad for the 5 cm transmit aperture.

3.3 Array size limits based on power requirements for timing recovery

The array size limits given in the previous section are based on estimates for the number of detector channels required to support the array, assuming a maximum of 144 detector channels supported by the current RealTOR FPGAs and channel combining architecture with minimal development (Section 4.1). For arrays of non-coplanar apertures, one must also consider possible additional power requirements needed per array element to track slot

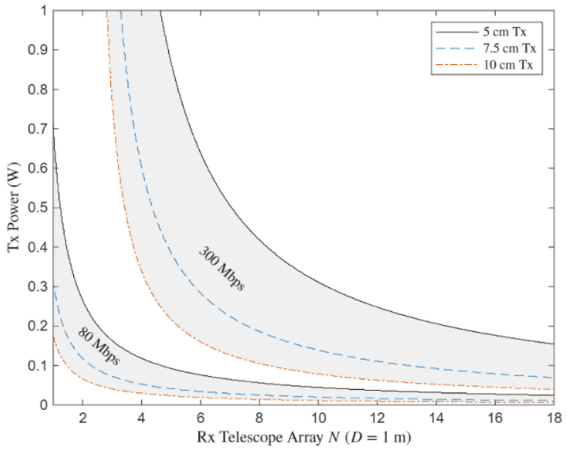


Figure 20: Data rate dependence on transmit power and array size for 1 m array from 0.01 AU.

phase differences. These slot phase differences arise from optical path length differences that occur when the apertures do not lie in a single plane normal to the optical axis of the array. Different techniques for tracking these slot phase differences will generally place different requirements on the power needed per array element (discussed in Section 4.1). Depending on the power per array element needed for timing recovery, this may place limits on the number of array elements that can be synthesized, as each additional element further divides the power needed to close the link at a desired data rate, yielding less power per array element to run the slot phase tracking algorithm.

Figure 21 shows the minimum signal photons per symbol per array element (before super-symbol aggregation) needed to close the link assuming 1 dB implementation loss and 1 dB fading loss for PPM orders M=8 to 128 and code rate 1/3. This minimum is largely independent of PPM order (two neighboring curves are plotted for each Q, corresponding to the maximum and minimum over all M) but is reduced proportionally to the number of repeated symbols per super-symbol Q, and the number of array elements. To fully support the number of array elements on the horizontal axis, the array timing recovery algorithm must be able to operate at the corresponding signal level per array element shown on the vertical axis. Here, we define an array element as any set of co-planar receive apertures, so, e.g., multiple telescopes can be combined into a single array element by placing them in a single-gimbal mount.

RealTOR receiver testing has shown timing recovery at K_s down to 0.05, as indicated by the dashed horizontal line. It should be noted that there may be techniques for tracking these geometrically induced slot phase differences which do not depend on the signal power per array element, and hence the ability to track would be independent of the size of the array; however, any such techniques remain to be demonstrated for optical PPM receiver arrays. Joint synchronization techniques as in [7] may also reduce the minimum K_s per array element needed for array timing recovery.

For modes without symbol repeat (Q = 1), full array timing recovery may be achieved at the minimum power needed to close the link for up to ∼20 array elements using demonstrated joint synchronization techniques [8]. For demonstrated slot widths up to 8 ns, the 114 kbps mode using an 8 ns slot requires symbol repeat Q = 16 (PPM-128, T_s = 8 ns, Q = 16, CR=1/3) and would not be supported with more than 1 array element.

The use of symbol repeat for the 114 kbps mode is only necessitated by assuming a maximum slot width of 8 ns. Alternatively, array timing recovery for the 114 kbps mode could be achieved for up to ∼20 array elements by employing a slot width of 128 ns with PPM-128 (Q = 1), which is within the maximum slot width of 512 ns included in the CCSDS HPE recommended standard [9]. The figure illustrates how the use of symbol repeat to achieve an effectively longer slot cuts into the power margin available to run the timing recovery loop at the shorter slot width. For a single array element, there is enough tracking margin at link closure for symbol repeat up to Q = 16; however, this same margin may also be needed to run a joint synchronization algorithm over many

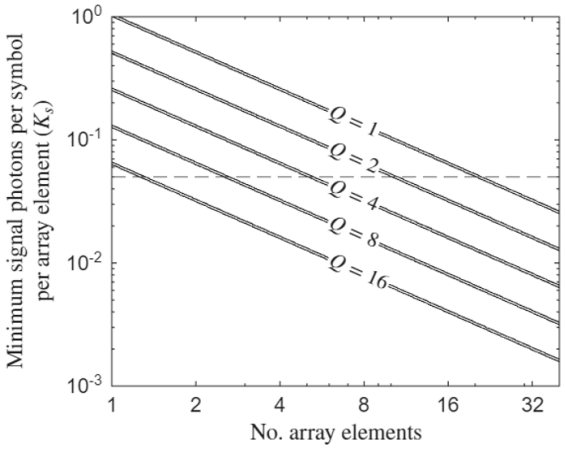


Figure 21: Minimum signal photons per symbol per array element needed to close the link for PPM-8 to PPM-128 and code rate 1/3. Two curves are plotted for each symbol repeat factor Q corresponding to the maximum and minimum over all $M \leq 128$. An array element is defined as any set of co-planar receive apertures, possibly including multiple telescopes on a single gimbal.

array elements, motivating a more complete investigation of the ability to achieve the longer slot clocks needed to avoid signal aggregation with symbol repeats.

3.4 Noise limits on photon counting arrays for low-rate deep space links

Another fundamental limit on the extent to which the RealTOR architecture can support expanded arrays is imposed by the dark counts that accumulate with each additional detector, as well as the added background from the spatial modes coupled to the detectors in direct proportion to the total collecting area. These limits impose a minimum on the supported data rates, as the higher order PPM modes used to accumulate enough power for photon counting over low-flux deep space links also yield a higher number of background photons per slot, K_b, given the same absolute background/dark count rate. Once the background counts per slot exceed $K_b \sim 0.01$, the performance of the timing recovery loop may start to degrade leading to implementation losses that negate the gain achieved by expanding the collecting area.

Figure 22 shows the minimum data rate allowing a maximum K_b of 0.01, based on the dark count rate per detector and the total number of detector channels. Note that for the 114 kbps mode, assuming dark counts no less than 400 cps, the dark count rate limits the number of detector channels to ∼200 detector channels, showing that dark counts also limit the number of detector channels independent of the channel combining constraints of the FPGA-based receiver architecture.

Figure 23 shows the dependence of the minimum data rate on total background radiance and total collecting aperture area $A = \pi N D^2/4$, assuming a 0.1 nm bandpass filter and a maximum $K_b = 0.01$. Here, we assume the total number of background spatial modes that must be coupled to the detectors scales as $M = 1.25 \cdot N(D/r_0)^2$, which keeps the estimated worst-case fiber coupling loss below 2 dB. Although night sky radiance is on the order of 10^{-8} W/(cm^2 sr μm), typical worst-case daytime sky radiance is around $2.5 \cdot 10^{-3}$ W/(cm^2 sr μm). Observe that even with 0.1 nm filtering, daytime operations are not supported for the lowest data rate modes, e.g. 114 kbps using PPM 128 with 8 ns slot width and symbol repeat 16, at least with the conservative requirement of $K_b \leq 0.01$ needed to achieve optimal receiver performance in system testing. Although tighter spectral filters have been demonstrated, one cannot push the filter bandwidth below ∼0.01 nm for an 8 ns slot, as this requires a 1 GHz filter with minimum photon coherence time of 1 ns, which is close to the maximum that can be accepted with an 8 ns slot width. In addition to the challenges inherent in the implementation of a 1 GHz filter, orbital speeds around Uranus can be as large as 16 km/s with a ∼3-hour orbital period, corresponding to up to 10 GHz doppler shifts on a 1550 nm carrier, such that a 1 GHz filter would also need to be tunable to actively track the received carrier frequency.

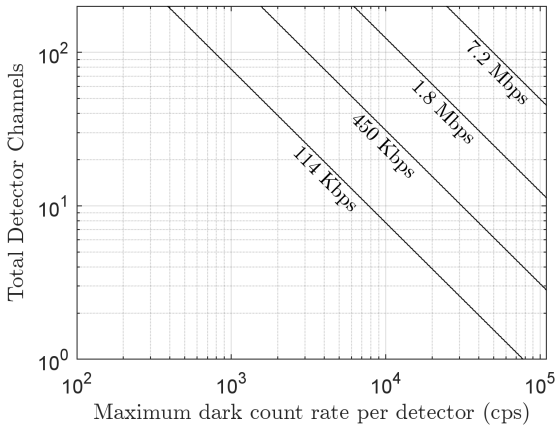


Figure 22: Maximum dark count rate per detector for low data rates based on a maximum $K_b = 0.01$ including PPM up to order 128 with symbol repeat up to 16.

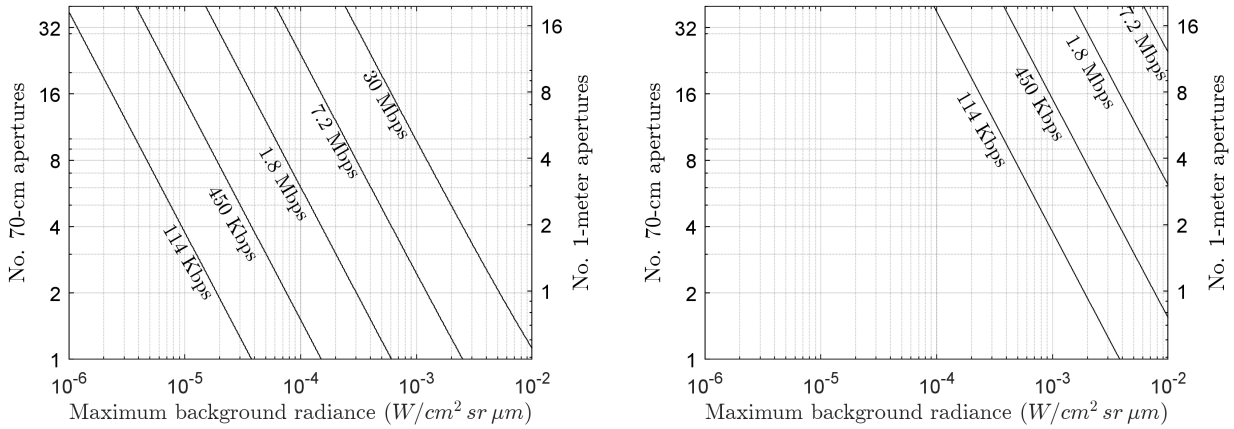


Figure 23: (Left) Maximum background radiance for low data rates based on a maximum $K_b = 0.01$ assuming a 0.1 nm bandpass filter for PPM ≤ 128. (Right) Maximum background radiance for low data rates based on a maximum $K_b = 0.1$ assuming a 0.01 nm bandpass filter for PPM ≤ 128.

Note that even with tight spectral filtering, the 114 kbps mode does not support more than one 70-100 cm aperture during worst-case daytime sky radiance of $2.5 \cdot 10^{-3}$ W/(cm^2 sr μm). This can be understood by explicitly accounting for the background modes entering the system as follows. The worst-case sky radiance translates directly to a mean photon number per mode $\mu_b \sim 2 \cdot 10^{-6}$. Thus, the system can accept at most 50,000 modes per slot before reaching the optimistic limit of $K_b \simeq 0.1$. Even with 1 GHz filtering (0.01 nm), there are ∼128 temporal modes per 128 ns slot. For a 1-m telescope, one can expect worst-case daytime turbulence with $D/r_0 = 20$. To efficiently couple this light without adaptive optics requires $M \sim 1.25(D/r_0)^2 = 500$ spatial modes per telescope per polarization, resulting in a total of $\sim 2 \cdot 500 \cdot 128$ =128,000 optical modes per slot, or ∼64,000 modes with polarization filtering, already exceeding the background count limit with just one telescope. Although there do exist techniques for filtering down to a single time-frequency mode, e.g. the quantum pulse gate [10], mode-matching the incoming pulses puts strict non-standard requirements on the coherent temporal modes of the PPM pulse train, and it is not yet known if these techniques can be adapted to a PPM pulse format. Thus, the most likely path towards full daytime operations for the lowest data rate links would be through some type of adaptive optics to reduce the number of spatial modes per telescope which must be coupled to the detectors. Noting that atmospheric tilt compensation can provide at most 2 dB of background suppression for

systems designed to operate at $D/r_0 \geq 14$ (see 3.1.4), the suppression needed to achieve daytime operation of the lowest data rates (114 kbps) would require a full adaptive optics solution. A consideration of adaptive optics solutions for a link with such extremely low signal flux is beyond the scope of this work, but at the least can be expected to add significant cost and/or complexity to ground station development and operations. On the other hand, in Section 3.5 we show that even restricting to nighttime operations for the low data rate modes one can still attain greater than 50% availability with 3-6 ground sites. Thus, in this study we focus on a ground station architecture based on the current RealTOR receiver with no adaptive optics assuming nighttime only operation for the lowest data rates as imposed by the background limits presented in the figures above.

Finally, it should be emphasized that the background noise limit is only relevant for the lowest data rate modes. Alternatively, a link designed to target higher data rates will automatically overcome the background limits as shown in the figures, enabling the full capability of large receiver arrays for daytime operations. However, these higher data rate modes can only be achieved by targeting a proportionally higher transmit power (EIRP) relative to the DSOC transmitter. These background limits demonstrate the asymmetry between scaling transmit power and receiver array size, showing that full daytime operation requires a transmit power (EIRP) sufficient to achieve the higher data rates from the target distance at which daytime operations are desired.

3.5 Operational limits based on Sun-Earth-Probe and Sun-Probe-Earth angle

The strict filtering requirements and additional receiver development needed to achieve daytime operation for the 114 kbps mode motivates a more careful consideration of the availability that can be achieved assuming only night operations. Sky radiance generally drops by 4-5 orders of magnitude during twilight, as the sun drops from 0° to 18° below the horizon. For a single ground station, restricting to elevation angles above 10°, the daily availability changes throughout the year with maximum availability during solar opposition when the Sun-Earth-Probe (SEP) angle is near 180° and little to no availability for 2 months during conjunction when the SEP angle is near 0° (Figure 24). Figure 24 shows an approximation of the daily availability for an equatorial ground station assuming operations start at 9° and 18° solar depression angles, respectively, not including unavailability due to clouds/weather. With additional ground stations, the total yearly average availability increases to a maximum of ∼89%; as there are ∼6 weeks during conjunction for which there are no locations on Earth that can link with Uranus at night with elevation angle above 10°. For two ground stations on opposite sides of the Earth the availability for night operations doubles, as they have no common link window, and there is also relatively little overlap with 3 well-spaced ground stations, which can reach an average availability of 55% (excluding weather). Additional ground stations provide diminishing gains in terms of availability for night-only operations (but provide critical redundancy for weather conditions including clouds).

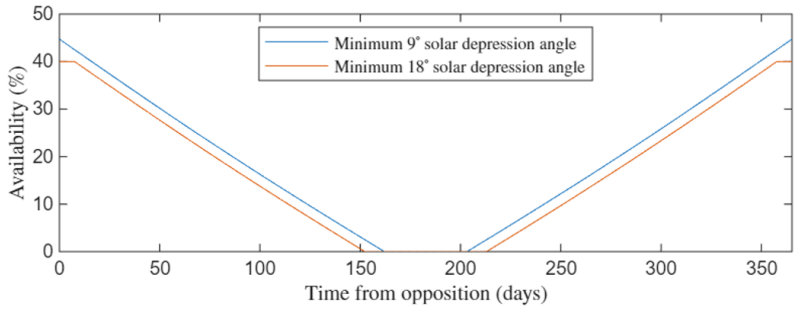


Figure 24: Approximate daily availability of a single equatorial ground station for nighttime operations for links with elevation above 10°.

Figure 25 shows the Sun-Probe-Earth (SPE) angle for Uranus ephemeris generated assuming a 4-year operation in orbit around Uranus. It is worth noting that the SPE angle remains below 3°, which may result in significant challenges for the uplink beacon used for downlink pointing in prior DSOC missions. A proper treatment of beacon requirements is beyond the scope of this study, but a full consideration of uplink beacon requirements versus beaconless pointing solutions [11] may be needed.

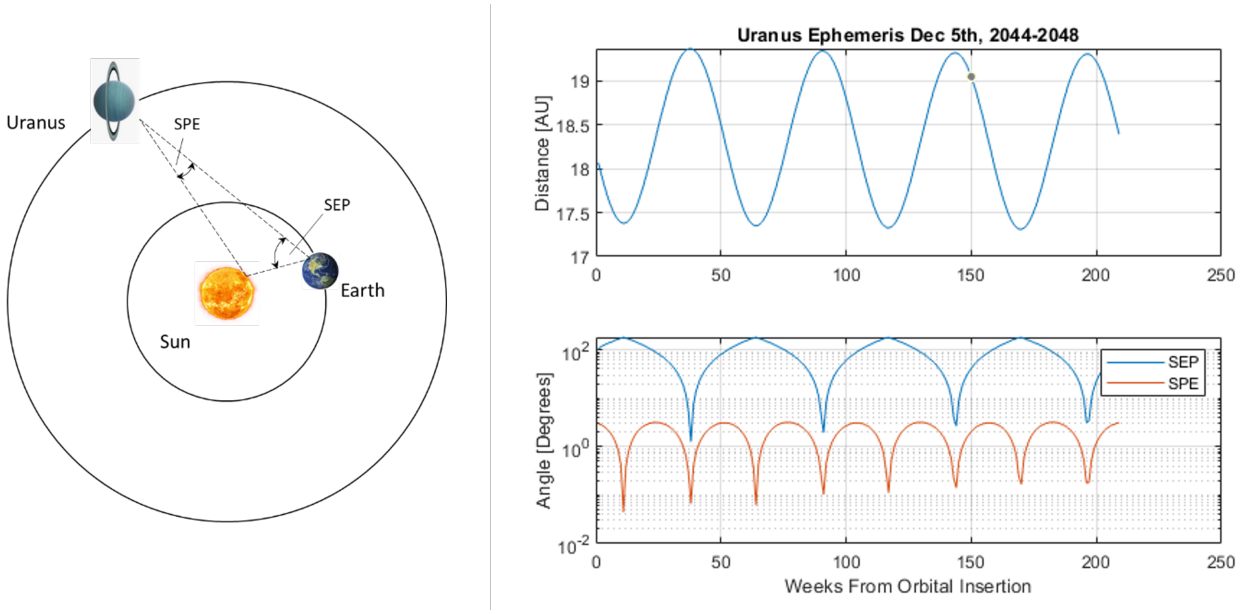


Figure 25: Diagram of separation angles Sun-Earth-Probe and Sun-Probe Earth (left). Uranus Ephemeris distance (top right) and SEP/SPE angle plots (bottom right).

4. RECEIVER TECHNOLOGY DEVELOPMENT

This section discusses the receiver technology that will need development.

4.1 Receiver Modem and Detector Channel Combining

The RealTOR system was demonstrated using a single RFSoC FPGA for timing recovery and detector channel combining and an additional FPGA for SCPPM decoding. The RealTOR modem chassis was designed to combine up to 64 detectors with a 125 ps slot and 3 photon counts per slot. It uses RFSoC FPGAs with 16 ADCs per FPGA each with a 2 GHz sample rate. The ADCs are time aligned using the multi-tile synchronization process developed by AMD. The delays introduced by varying fiber optic and RF cable lengths are compensated for using digital phase shifters in the FPGA. The limiting factor in the number of channels is the number of backplane ports in the uTCA architecture and the number of gigabit transceivers implemented on the RFSoC FPGA.

However, the backplane can be reoptimized in a way to maximize the number of detector channels combined for a 500 ps slot clock. Figure 26 shows the clocking and commanding diagrams. Figure 26(a) shows the clocking diagram. Each FPGA board is synchronized to a common 10 MHz reference. The multi-tile synchronization program aligns ADC channels within a single FPGA and the digital phase shifters can be used to compensate for different delays across the FPGA boards. Figure 26(b) shows the commanding diagram. An external commanding interface sends commands to reset and enable the master FPGA, which then passes the commands over multi-point LVDS to the other FPGA boards. Figure 27 shows the data flow diagram. Each FPGA contains a front end which resamples the input signal from the detectors, performs photon counting and channel combining, the digital phase shifting, and then sends the data over a high-speed serial link to the master FPGA which implements all of the functions of the timing recovery loop. It sends the control loop feedback signal to each slave FPGA to maintain timing synchronization. After timing recovery, codeword alignment, and deinterleaving, the slot statistics are sent to the decoder FPGA for SCPPM decoding. With this architecture, it would be possible to use 9 RFSoC FPGAs to sample and combine a maximum of 144 detector channels. If all 144 channels are not needed, the architecture is scalable to using less detectors. Additionally, if FPGAs with more ADCs on the chip were available, the number of detector channels could be increased. In this case the limiting factor may be the performance loss incurred due to combining so many detector channels.

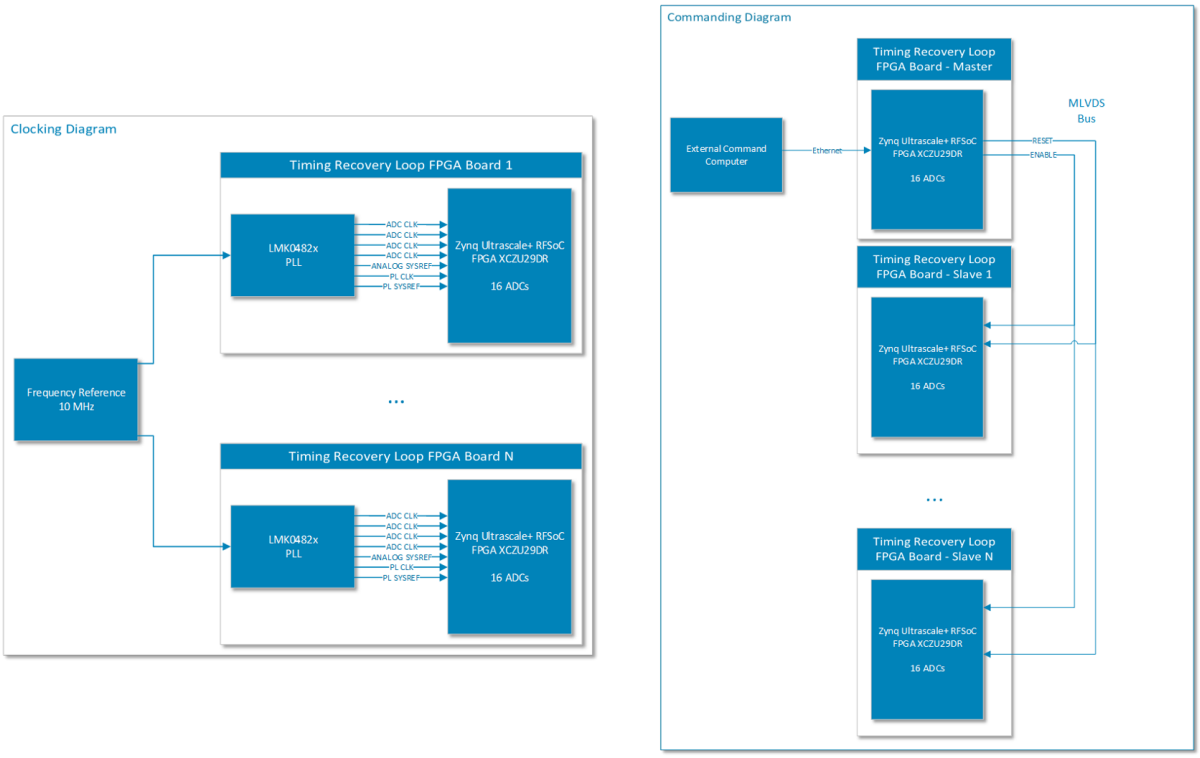


Figure 26: Clocking (a) and commanding (b) diagrams for a receiver architecture which combines up to 144 detector channels.

The current RealTOR timing alignment method uses the timing recovery loop to determine the relative slot phase offset of each detector channel when the transmitter and receiver clocks are locked. The result is used to set the initial values of the digital phase shifters. In a ground station with arrayed telescopes, this could be implemented by having the test transmitter located centrally next to the receive modem and a fiber-optic distribution of the test signal to each telescope. This signal could be injected into a test port of the backend optics in the telescope. By using this method, the system will be aligned when the telescopes are pointed at zenith, but there will be significant timing offsets otherwise. A method presented in [7] uses joint independent synchronization to compensate for timing offsets while the communications link is running, but the lower bound on the necessary K_s for tracking each telescope would eliminate some of the array gain while using symbol repeat modes. A second option would be to develop a method to characterize the delays over the full range of azimuth and elevation angles and compensate for them using the digital phase shifters. Therefore, the signal from all the telescopes would be aggregated prior to performing timing recovery, which could enable a lower K_s per aperture. Additionally, a telescope gimbal holding multiple apertures would reduce tracking constraints for both methods as the telescopes mounted on the same gimbal would be in the same plane and so the signal could be aggregated prior to processing.

4.2 Fiber interconnect

The RealTOR receiver was designed around fiber delivery of the light from the collection aperture to the detectors. This design was chosen to accommodate the COTS SNSPDs. Using fibers offers flexibility in the configuration and physical placement of the equipment enabling options that can lower costs and maintenance. Specifically, in the telescope arraying concept of the receiver explored in this study, using fibers enables the reduction of the number of cryostats for the SNSPDs thereby reducing the cost and maintenance of the system. Although using fibers has overall design benefits, it introduces losses from mode coupling and increases timing jitter through mode and material dispersion. Mode coupling losses are driven by turbulence in Earth's atmosphere, where

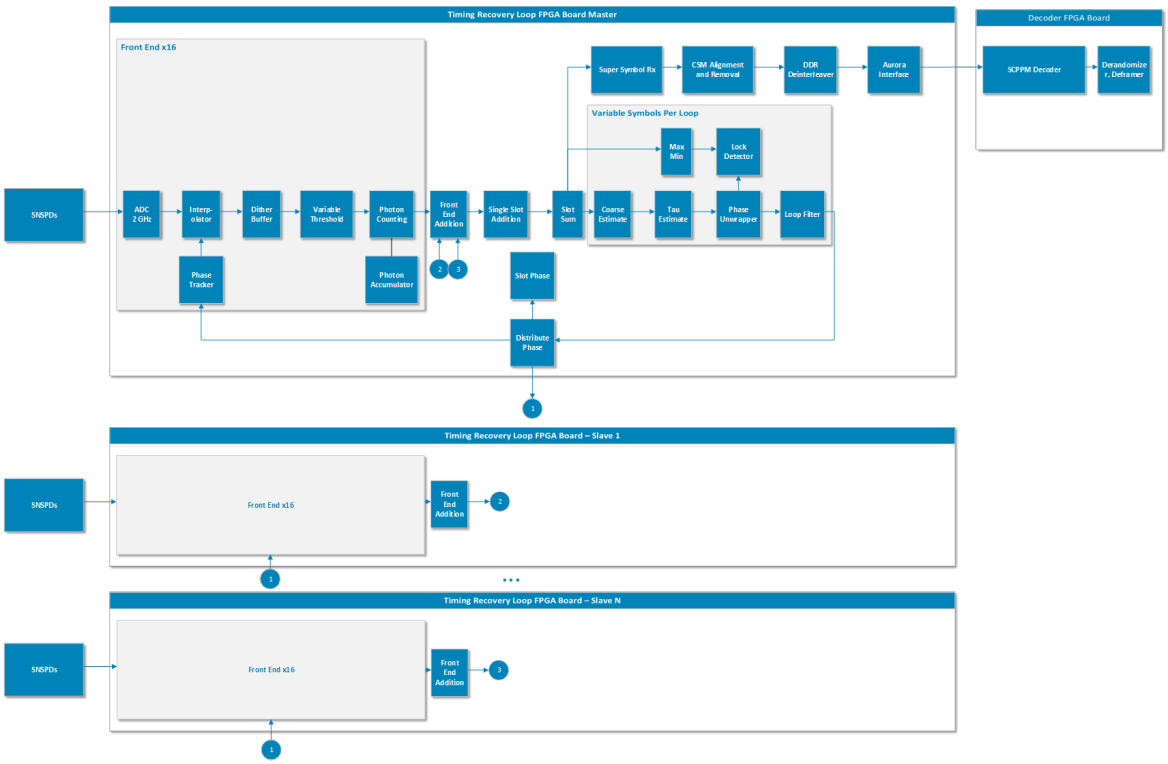


Figure 27: Data flow diagram for a receiver architecture which combines up to 144 detector channels.

random refractive index fluctuations cause the light to become blurred into many spatial modes at the focal plane of the telescope. By using a fiber with enough mode capacity to collect light from most of the modes populated by this atmospheric blurring, the mode coupling losses can be minimized as shown by Eq. 14 and Figure 11 in Section 3.1.4. The mode capacity of a fiber is determined by the refractive index profile and increases with the core diameter and the numerical aperture (NA). However, the amount of background light collected scales directly with the number of modes coupled into the fiber. As seen in Fig. 11, increasing the number of modes has diminishing returns in signal coupling beyond a certain threshold. For example, for the $D/r_0 = 15$ curve, after ~500 modes are coupled there is relatively little additional gain by adding more modes but each mode adds background light and therefore the signal-to-noise ratio (SNR) generally decreases. We set the target mode capacity to $1.25(D/r_0)^2$, which estimates the onset of saturation in coupling efficiency at $\eta_{\text{fib}} \simeq 1 - e^{-1}$. Adding more modes into the saturation regime can improve the achievable data rates for low-noise links with excess SNR, but also adds background faster than signal reducing the SNR and impacting the lowest data rate supported by the array at a fixed background radiance.

The core diameter size and the numerical aperture impacts the SNSPD requirements and the overall jitter budget for the receiver system. Minimum fiber-to-detector coupling loss is achieved when the fiber core diameter and SNSPD size and shape match. The fiber NA and index of refraction profile determines the modal dispersion. Larger NAs increase the modal dispersion. A parabolic index of refraction profile, referred to as graded-index, typically reduces the modal dispersion by a factor ~100. Modal dispersion accumulates over the length of the fiber creating timing jitter. The amount timing jitter that can be contributed from the fiber is limited by the timing jitter contributions of the detectors and electronics and the desired error rate performance. For this study we assume the fiber can contribute up to 20% of the 500 ps slot width or 81 ps full-width-half-maximum (FWHM).

To implement the telescope array, the signal from the telescopes must be combined. One way to combine the signal is by adding the light together before it reaches the detectors as shown in Fig. 1. There are several challenges to implementing this solution. The first challenge would be the timing alignment as each fiber channel

would have to be aligned in time with ∼50 ps precision. This could be implemented with delay lines either in the backend optics or in fiber. These delay lines would need to be actively controlled with a feedback loop as changes in temperature and mechanical fiber bends would impact the timing of the light arriving on the SNSPD. This control loop would have to be implemented using the SNSPDs and FPGAs. Due to the photon counting operating regime the SNSPDs and FPGAs would have to perform this control loop as well as timing recovery and decoding simultaneously. This control loop may not be feasible or practical to implement as the increase to the complexity, cost, and maintenance of the system would be substantial. The second challenge is combination of the light from the fibers into a fiber with a large enough mode capacity to support all the modes from each fiber. To support the combination of these modes the core diameter of the output fiber device would be at least 2-4 times larger than the input core diameters to combine the light from 4-16 fibers. This increases the requirement on the active area of the SNSPDs proportionally to the number of combined fibers.

Another way to combine the signal is digitally as described in Section 4.1. In this concept, shown in Fig. 2, each fiber connects from 1 telescope aperture to an SNSPD array. While this concept introduces a 1-to-1 relation between the telescope apertures and SNSPD fiber inputs, it requires less development and control loop engineering for the optical hardware. Here we propose fiber solutions for the 70 cm, 1 meter, and 2.5 meter telescopes.

First, we will identify a fiber solution that could be implemented with the least amount of development to the RealTOR technology for the array of up to 18, 70 cm telescopes. To avoid adding excess background, we target a fiber with 245 spatial mode capacity at the coupling saturation limit $1.25(D/r_0)^2$, allowing up to a 1.8 dB loss at a worst case D/r_0 of 14. This loss will be reduced significantly at nominal and best case D/r_0. A common COTS fiber is available that can support 248 spatial modes with a 100 micron core, and 0.22 NA. This fiber requires a factor of four increase to the SNSPD area as compared to the existing RealTOR COTS SNSPDs, a 50 micron array developed under an SBIR. This SNSPD development is discussed in Section 3.1.6. The 0.22 NA would add ∼0.16 ps of jitter for every meter of length. Assuming the fiber can only contribute 81 ps of jitter, the fibers can be up to 240 meters long. This restricts the distance between the telescopes, domes, and supporting building. For example, Fig. 28(a) shows a configuration assuming the fibers will be run to a cryostat in a building located in the middle of up to 18 telescope domes arranged in a circle packing configuration. If instead of using 1 gimbal per telescope, a 4-aperture gimbal mount is used as discussed in Section 4.1 then the layout would be as shown in Fig. 28(b). For the layout in Fig. 28(a) the centers of the domes can be no more than ∼107 meters apart, or ∼210 meters for the case in Fig. 28(b). There is potential for the length restriction to be reduced or eliminated through the development of a special fiber such as a hollow core fiber.

Note that the minimum spacing between neighboring domes is 11 meters in (a), or 22 meters in (b), to ensure unobstructed views of the spacecraft down to an elevation of 10°. This assumes 5-meter domes such that the bottom of each telescope aperture is ∼2 m and ∼4 m below the top of the neighboring dome for (a) and (b), respectively. The building roof is assumed to be no higher than the dome height. Fig. 28(a) and (b) shows the minimum spacing.

Next, we consider the 1-meter telescope solution. Assuming a nominal worst-case of D/r_0 of 20, we target a fiber with 500 spatial mode capacity resulting in average worst-case performance allowing up to a 1.9 dB loss. As discussed in Section 3.2, a reasonable target for the SNSPD area using a limit of 144 channels for a 1 m telescope is 100 microns. To reach the 500 mode capacity, the NA would need to be increased to 0.32. This fiber would have to be developed as the closest COTS fiber is a 100 micron core with a 0.29 NA. The 0.32 NA would add ∼ 0.68 ps of jitter for every meter of length. Assuming the fiber can only contribute jitter 81 ps then the fibers can be up to 120 meters long. As discussed above for the 70 cm diameter, this restricts the distance between the telescopes domes and supporting building. To support up to 18 telescope domes as above, the center of the domes can be no more than ∼25 meters apart for the case in Fig. 28(a). If 5 domes with 4-aperature gimbals are used as in Fig. 28(b), then the domes can be up to ∼90 meters apart.

Finally, for a telescope aperture of 2.5 meters at a nominal worst-case D/r_0 of 50, we target a mode capacity of 3125 allowing up to a 1.9 dB loss. Commercial fibers closest to this mode capacity are step index fibers with 300-micron diameter cores and a 0.39 NA. But a step index fiber would add ∼80 ps/m, meaning these fibers would exceed the jitter requirement of 81 ps in just 1 meter. Typically, there are 2-3 meters of fiber internal to the SNSPDs alone, not to mention the length of fiber needed to reach the back-end optics of the telescope.

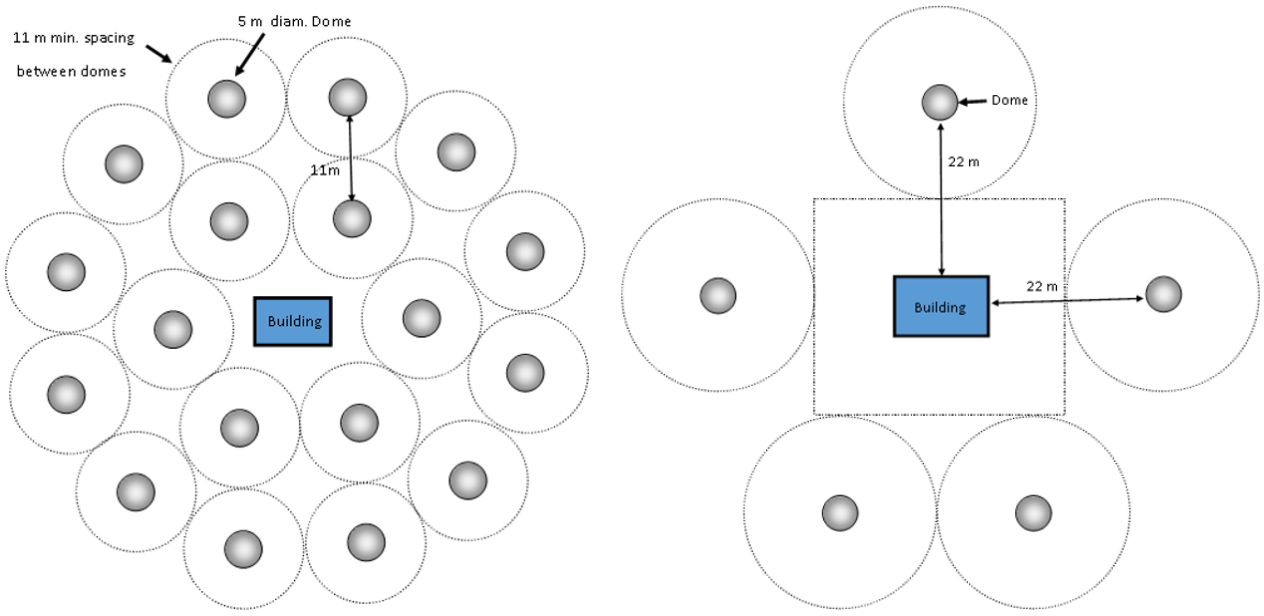


Figure 28: Configuration of domes with minimum spacing allowed for clear of view at 10 degrees elevation for every telescope: (a) for 18 domes for the 70 cm and 1-meter telescope apertures and (b) 5 domes 70-100-cm apertures on combined 4-aperture gimbals or the just the top 3 domes for the 2.5 telescope aperture.

Therefore, new graded index fiber would need to be developed to reduce the timing jitter. To keep to the SNSPD/channel numbers assumed in Section 3.2 the core would need to be ∼250 μm. A ∼3200 mode capacity can be reached with 0.32 NA. This fiber would need to be developed. Based on the analysis in Section 3.2 the maximum number of telescopes needed would be 3. Assuming only the top 3 domes shown in the Fig. 28(b) arrangement, the maximum separation of the domes would be 56 meters. In Fig. 28(b) the minimum spacing is shown based on unobstructed viewing at 10 degree elevation, i.e., 22 meters for the 2.5 meter aperture.

5. SITE LOCATION FOR GROUND STATIONS

Northrop Grumman has previously developed the Lasercom Network Optimization Tool (LNOT) [12]. This tool has been used in NASA missions since 2008 to predict link availability. More recently NASA directed Northrop Grumman to do a study for site locations for a lunar mission. The study takes into account the link contact times, onboard data storage buffer, and the number of ground and the atmosphere properties of the ground stations. A similar study would need to take place to optimize coverage for the UOP mission. Figure 29 shows a geographically diverse network of ground sites to obtain 94.65 percent data transfer for an L1 space-to-ground link from [13]. The number of sites and locations are dependent on link geometry and cloud-free availability.

6. GROUND STATION NETWORK DEVELOPMENT ROADMAP

Assuming a start date of Oct. 1, 2025, the development of a ground station network capable of support the Uranus probe mission's would start with the design of a ground station array unit cell. A predicted roadmap is shown in Fig. 30. This roadmap assumes that all technologies would need no more than 3 years of engineering/technology development.

The component technology development would happen during the design, build, and integration phases of the first arrayed ground station. The telescope array, and downlink pointing design would start first as they will determine the SNSPD and fiber interface requirements. The modem channel combining development could start right away, followed by the full design after the SNSPD design is complete. The first ground station build begins with site selection and design. Following the preliminary design review (PDR) and critical design review (CDR),

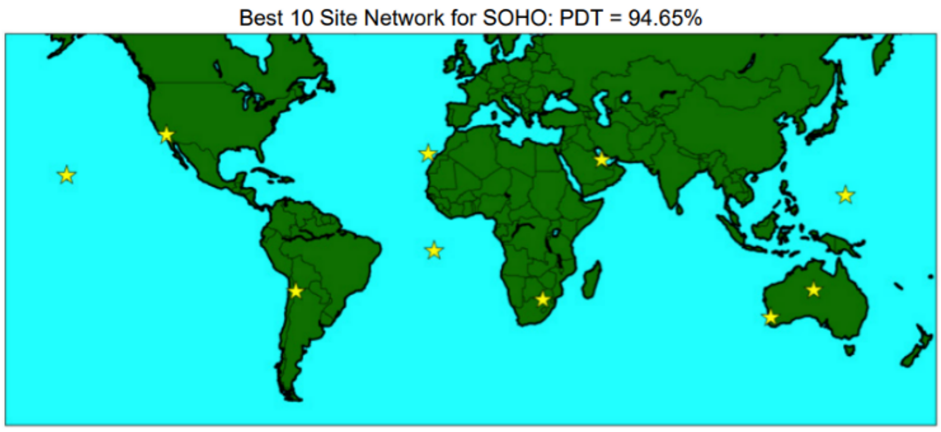


Figure 29: Locations for ground stations from [13].

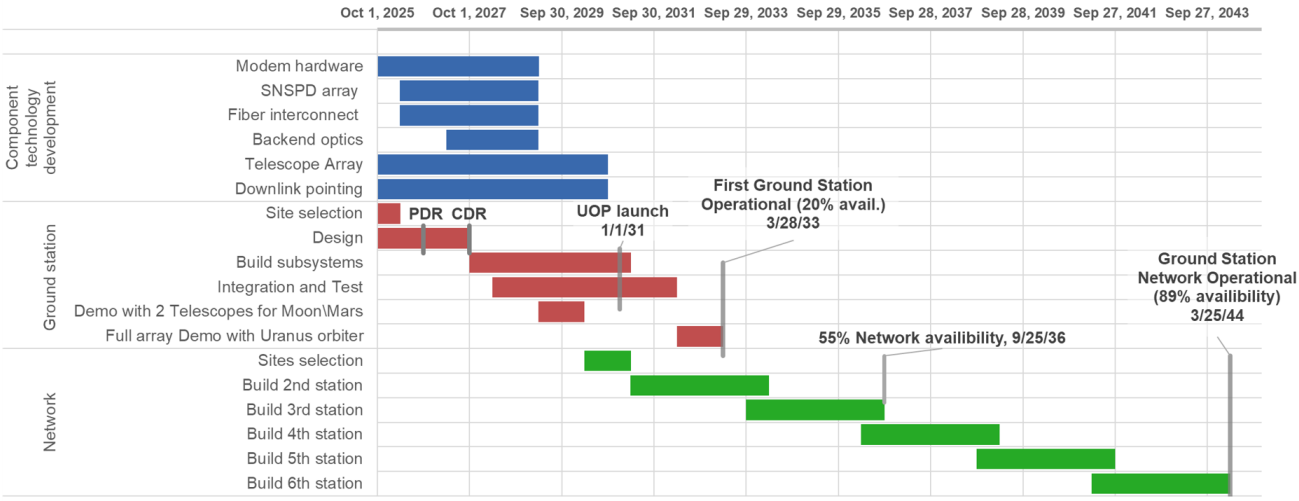


Figure 30: A roadmap to establishing a ground station network for the Uranus Orbiter Probe.

the subsystems would be purchased, and building would start in 2027. By 2028 subsystems would start to be integrated and tested. In 2029, a sub-element of the ground station array consisting of 2 telescope apertures in combination with the full modem receiver would be demonstrated with a Moon or Mars asset. This ground station could continue to serve as a ground station for Moon or Mars missions while the rest of the apertures were added to the array. By 2032 the first ground station array would be complete and ready for a demonstration with the Uranus Orbiter Probe scheduled for launch in 2031. If the UOP is not launched a demonstration can be performed with a Moon or Mars asset. This demonstration would make the ground station fully operational by 2033 and provide up to 20% availability to the UOP assuming nighttime operations and cloud free line of sight. After adding the next 2 ground stations, the network's nighttime availability would increase to 55%, excluding cloud coverage. Adding more ground stations would have diminishing returns for nighttime availability, with an asymptotic limit at 89% availability; however, the remaining ground stations would also enable redundancy for weather outages. A network of 6 ground stations can be achieved before the orbiter reaches Uranus in 2044 by building $\sim$1 station every 2.5 years.

7. POINT DESIGN DISCUSSION

This summary offers a study of an array receiver design for the UOP mission. The point designs considered were introduced in Section 3.2.1 with further receiver developments discussed in Section 4. The defining features of the subcomponents of each point design are summarized in Figure 31. Based on the recommendation from Section 4.2, all point designs assume digital recombining of the signal. Also assumed for all cases is a background filtering of 0.2 nm and nighttime only operation. The darker the shade of the box the more demanding the requirement is compared to the other entries in that column in Figure 31.

The quickest, cheapest path to a ground station network for the UOP would be built with existing COTS components that were developed and tested from previous NASA programs. Specifically, in this study we considered using the DSOC transmitter (22 cm and 4 W) with the LCOT (70 cm) and RealTOR technologies. Unfortunately, using these technologies unchanged would require over 50 apertures and many times more than the maximum practical limit of 144 detector channels. Therefore, instead Figure 31 offers alternative solutions in which the DSOC, RealTOR, or LCOT technologies are modified.

	Transmitter			Receiver				
Point Design	Power (W)	Aperture Size (cm)	Pointing Req. (μrad)	# of apertures	Aperture Size (cm)	# detector channels	Receive Fiber	Detector area
A	12	22	2.5	18	70	144	100 um, 0.22 NA	100
B	6	22	2.5	18	100	144	100 um, 0.32 NA	100
C	22	22	2.5	9	70	72	100 um, 0.22 NA	100
D	4	50	1.1	9	70	72	100 um, 0.22 NA	100
E	11	22	2.5	9	100	72	100 um, 0.32 NA	100
F	6	30	1.9	9	100	72	100 um, 0.32 NA	100
G	5	50	1.1	4	100	48	100 um, 0.32 NA	100
H	5	22	2.5	3	250	144	250 um, 0.32 NA	250
I	7	30	1.9	2	250	96	250 um, 0.32 NA	250

Figure 31: Summary of point designs from Section 3.2.1.

In point design A, we select the maximum number of detector channels to the challenging but reachable goal of 144. This sets the number of receive apertures to 18. Co-aligning and pointing 18 apertures simultaneously will require significant development and infrastructure establishment. This would also require the time alignment of 18 groups of signals requiring synchronization. The number of groups can be reduced by mounting multiple 70 cm or 100 cm telescopes on a single gimble reducing the number of signals to time align. A gimbal which holds four 100-cm telescopes is available from Planewave. In this case we increase the DSOC transmitter power by 3 times to 12 W to satisfy the link budget. This increase in laser power would increase the spacecraft power requirements and introduce challenges in fiber power amplification. In point design B we consider an option to reduce the transmit power by half to 6 W by increasing the receive aperture to 100 cm. A 6 W fiber laser was built by Fibertek as discussed in Ref. [14]. This solution will require custom fabrication of a receive fiber that has an increased NA compared to the COTS fiber used in design point A. Design point B maintains the same challenges associated to the many required apertures and detector channels as design point A.

Design point C offers a reduction of the number of 70 cm apertures to 9 and decreases the detector channels by about half to 72 compared to design point A. To satisfy the link budget, the transmitter power is increased by almost 2 times to 22 W. This may be an unfeasible increase in transmit power and will require significant increases of spacecraft power and development of the fiber laser amplifiers. Therefore, in point design D, we consider increasing the transmitter aperture instead to 50 cm (the size of HiRISE), allowing the reduction of transmit power to 4 W (equal to DSOC). Increasing the transmit aperture will decrease the pointing requirement by half, doubling the required precision. Point design E offers an alternative solution to the increase in transmit aperture from point design D, instead increasing the receive sub-aperture diameter to 100 cm, reducing the required transmit power to 11 W. Point design E's most demanding requirement, like A, is the almost 3 times

increase in transmit power from the DSOC baseline. Design point C and D both use a receive fiber that is COTS, where design point E requires the modified custom fiber.

In design point F we consider an intermediate transmit aperture size of 30 cm, which slightly increases the pointing precision requirement and increases needed transmit power from 4 W to 6 W. These transmit features enable a receiver array of 9 apertures of 100 cm with a total of 72 detector channels. This design point has no features with the most demanding requirements.

Design point G offers a solution that requires the least amount of detector channels by considering the use of the HiRISE 50 cm telescope with 100 cm receiver sub-apertures. This solution increases the pointing precision requirement to the most demanding and will add mass to the space transmitter, but only requires 4 receive apertures. Using the 4 aperture mount would simplify co-alignment procedures and would eliminate timing alignment needs discussed in Section 4.1. Another benefit of this design point is that it could be implemented with only 1 dome, reducing building needs.

Finally design points H and I consider a much larger receive sub-aperture of 250 cm. This telescope is COTS but it hasn't undergone development for optical communications. Design point H would allow the use of the DSOC transmitter and only requires 3 receive apertures. This solution requires the maximum detector channels and the development of a custom graded index fiber with a core much larger than any COTS fibers. Since the transmitter must be completed well before launch of the UOP this solution could be the most feasible. If the transmitter aperture and power are allowed a few years of development before integration into the UOP then design point I would offer a reduction of the number of apertures to 2 and detector channels to 96 compared to H. Since more time would be available for the ground network than the transmitter, solutions H and I may be feasible.

In summary, the best receiver solution is highly dependent on the transmitter power and pointing capabilities attainable before the launch of the UOP. Because the transmitter must be integrated on the spacecraft its requirement for completion is much earlier than the receiver. Design points A, C, D, E and G would be challenging to implement in a less than 3 year build available for the transmitter based on the 2031 launch date. Design point F, B, H, and I are reasonable alternatives if the most demanding transmitter requirements can not be met. If the spacecraft can handle the increase to a 50 cm aperture and the pointing accuracy is achievable then design point G offers a receiver solution with the least amount of channels, eliminates timing alignment challenges, and reduces the number of domes to 1.

8. SUMMARY

We described concepts for a deep space optical communications ground receiver array, based primarily on NASA GRC's RealTOR system and available or near-term COTS components. While certain key transmitter and receiver elements were considered in detail, further assessments of engineering trades between receiver requirements and transmitter flight subsystem technologies will need to be conducted. In particular, at Uranian distances tracking and pointing will present new challenges as it may not be feasible to supply an uplink beacon to $\sim$19 AU from Earth, and other possibilities such as tracking using Earth imaging may be limited due to SPE angles $\lesssim 3^\circ$ at all times. Beaconless pointing using star-trackers may prove to be the most viable alternative in this scenario. A more complete analysis of additional transmitter development that can be pursued to reduce the ground station requirements outlined in the point design (i.e. further developing the trade study performed in Section 3.2 with a focus on transmitter capabilities) is necessary for a full recommendation on the optical link architecture. Other supporting considerations such as networking and infrastructure development will need to be addressed as well.

ACKNOWLEDGMENTS

This work was funded by NASA's Science Mission Directorate. We would like to thank Bernie Edwards and Carolyn Mercer for their suggestions.

REFERENCES

[1] Klein, B. J. and Degnan, J. J., "Optical antenna gain. 1: Transmitting antennas," *Appl. Opt.* **13**, 2134–2141 (Sep 1974).

[2] Chahine, Y. K., Tedder, S. A., Staffa, J., and Vyhnalek, B. E., "Optimal efficiency for passively coupling partially coherent light intomode-limited optical waveguides," *J. Opt. Soc. Am. A* **38**, 1732–1743 (Dec 2021).

[3] Chahine, Y. K., Rushton, F., Vyhnalek, B. E., and Tedder, S. A., "Numerical phase space optics methods and applications to the analysis of fiber coupling efficiency in atmospheric turbulence," in [*Free-Space Laser Communications XXXIV*], Hemmati, H. and Robinson, B. S., eds., *Society of Photo-Optical Instrumentation Engineers (SPIE) Conference Series* **11993**, 119930U (Mar. 2022).

[4] Hemmati, H., [*Deep Space Optical Communications*], John Wiley and Sons, Hoboken, New Jersey (2006).

[5] Thorne, K. S. and Blandford, R. D., [*Modern Classical Physics*], Princeton University Press (2017).

[6] Downey, J. N., Chahine, Y. K., Tedder, S. A., Katz, E. J., Marsden, M. A., and Clapham, J. S., "Performance of a real-time photon counting optical receiver in the presence of emulated channel fading," in [*Free-Space Laser Communications XXXVI*], Hemmati, H. and Robinson, B. S., eds., **12877**, 128770Z, International Society for Optics and Photonics, SPIE (2024).

[7] Rogalin, R., Cho, D., and Okino, C., "Architecture and analysis of telescope arrays for deep space optical communication," in [*Laser Communication and Propagation through the Atmosphere and Oceans XIII*], Anguita, J. A., Bos, J. P., and Wayne, D. T., eds., **13147**, 1314709, International Society for Optics and Photonics, SPIE (2024).

[8] Rogalin, R. and Xie, H., "Telescope arrays for deep space optical communications," in [*Free-Space Laser Communications XXXVII*], Hemmati, H. and Robinson, B. S., eds., **13355**, 133550Q, International Society for Optics and Photonics, SPIE (2025).

[9] CCSDS-141.0-B-1, [*Optical communications physical layer*], CCSDS (2019).

[10] Eckstein, A., Brecht, B., and Silberhorn, C., "A quantum pulse gate based on spectrally engineered sum frequency generation," *Opt. Express* **19**, 13770–13778 (Jul 2011).

[11] Swank, A. J., Aretskin-Hariton, E., Le, D. K., Sands, O., and Wroblewski, A., [*Beaconless Pointing for Deep-Space Optical Communication*] (2016).

[12] Alliss, R. J., "Optimizing the performance of space to ground optical communications," in [*Free-Space Laser Communications XXXI*], Hemmati, H. and Boroson, D. M., eds., **10910**, 1091006, International Society for Optics and Photonics, SPIE (2019).

[13] CCSDS-140.1-G-2, [*Real-Time Weather and Atmospheric Characterization Data*], CCSDS (2024).

[14] Engin, D., Litvinovitch, S., Gilman, C., Cao, H., Wysocki, T., McIntosh, B., Rudd, J., Hwang, J., Pachowicz, D., Petrillo, K., Sawruk, N., Schober, A., and Storm, M., "50W, 1.5um, 8 WDM (25nm) channels PPM downlink Tx for deep space lasercom," in [*Free-Space Laser Communications XXXIII*], Hemmati, H. and Boroson, D. M., eds., **11678**, 116780K, International Society for Optics and Photonics, SPIE (2021).